CHALMERS
UNIVERSITY OF TECHNOLOGY

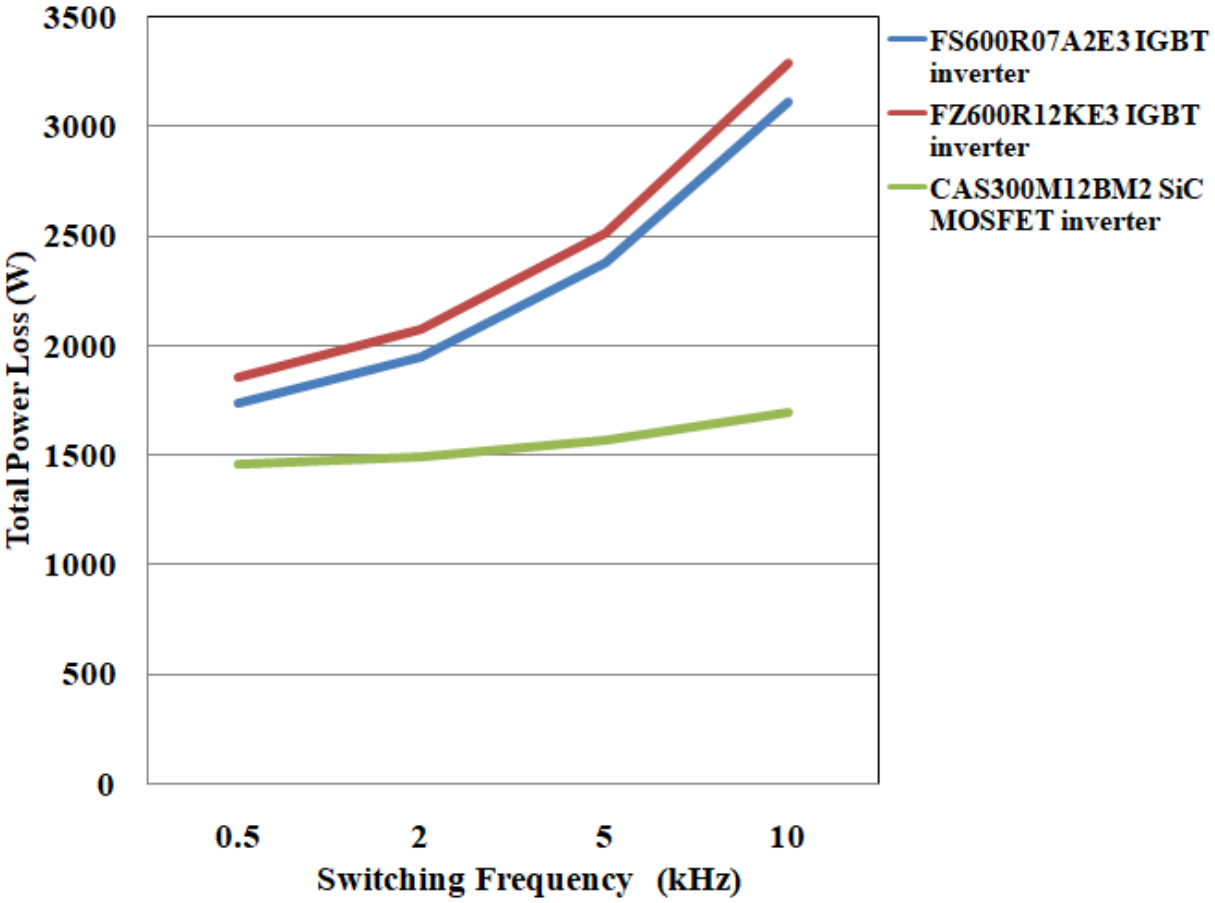

Loss Determination in IGBT/SiC Converters Using a Non-linear Permanent Magnet Synchronous Machine Model

Master's thesis in Energy and Environment

Manoj Saladi, Mubashar Bashir

Department of Electrical Engineering
CHALMERS UNIVERSITY OF TECHNOLOGY
Gothenburg, Sweden 2019

Master's thesis 2019

Loss Determination in IGBT/SiC Converters Using a Non-linear Permanent Magnet Synchronous Machine Model

Manoj Saladi, Mubashar Bashir

CHALMERS
UNIVERSITY OF TECHNOLOGY

Department of Electrical Engineering
Division of Electric Power Engineering
Chalmers University of Technology
Gothenburg, Sweden 2019

Loss Determination in IGBT/SiC Converters Using a Non-linear Permanent Magnet Synchronous Machine Model

Manoj Saladi
Mubashar Bashir

Supervisors: Sepideh Amirpour, Dan Hagstedt, CEVT AB
Examiner: Torbjörn Thiringer, Electrical Engineering

Master's Thesis 2019
Department of Energy and Environment
Division of Electric Power Engineering
Chalmers University of Technology
SE-412 96 Gothenburg
Telephone +46 31 772 1000

Typeset in LaTeX
Printed by [Chalmers University of Technology]
Gothenburg, Sweden 2019

Loss Determination in IGBT/SiC Converters Using a Non-linear Permanent Magnet Synchronous Machine Model
Manoj Saladi, Mubashar Bashir
Department of Energy and Environment
Chalmers University of Technology

Abstract

There is a growing requirement in the automotive industry to reduce the power losses in the conversion unit (Inverter) of the EV and hybrid power trains. The higher switching loss is a limiting factor for IGBT devices, which makes them unsuitable for high-frequency applications. SiC MOSFETs, however, seems like a promising alternative because of their lower switching energy loss when compared to IGBT inverters. Though reverse conduction in MOSFETs helps in the reduction of conduction losses, yet its rapid variation with respect to junction temperature is one of the disadvantages of SiC MOSFETs.

Therefore in this thesis work, power losses are compared for FS600R07A2E3 IGBT module, FZ600R12KE3 IGBT module and CAS300M12BM2 SiC MOSFET module, to investigate if SiC MOSFETs are worth replacing the widely used Si IGBT modules in the power conversions units. The whole power loss comparison is made for one of the operating points of a permanent magnet synchronous machine, where the details of it are provided in this report. To obtain the power loss values, which are more closer to reality, the non-linearity is included in the permanent magnet synchronous machine by using the non-linear d and q-axis flux maps of the machine. The power losses in the power converters are calculated after the implementation of the third harmonic injection PWM and are compared with the power losses calculated by using a pure sinusoidal reference voltage PWM.

Life-Cycle Cost analysis (LCCA) is performed for both the CAS300M12BM2 SiC MOSFET inverter and the FZ600R12KE3 Si IGBT inverter. Initial cost and energy cost analysis are performed by taking the discount rate into consideration. The LCCA model is derived from calculating the total cost over the defined lifetime of the power converters.

In the power loss calculations it was observed that, at 0.5kHz switching frequency, the power losses of the SiC MOSFET inverter are 21% lower compared to that of the FZ600R12KE3 IGBT inverter, whereas this difference has increased to 48% at 10kHZ switching frequency. In the high-cost scenario, the LCCA model developed, has shown that the usage of a SiC MOSFET inverter becomes advantageous after around 21 years. However, it was seen that in the low-cost scenario, a SiC MOSFET inverter has a clear advantage over the IGBT inverter just from the time of installation or usage.

Keywords: PMSM, MTPA,MTPV, IGBT, SiC MOSFET, LCCA, THIPWM, ECE, NPV, Conduction power loss, Switching power loss, Total power loss.

Acknowledgements

First of all, we would like to thank Chalmers University of Technology and China Euro Vehicle Technology AB for giving us this thesis work opportunity.

We want to thank our supervisor and examiner at Chalmers, Torbjörn Thiringer, for his guidance throughout the whole thesis work. We acknowledge our supervisor at CEVT AB, Sepideh Amirpour, whose suggestions were beneficial in inverter loss calculations. Thanks to our other supervisor at CEVT AB, Dan Hagstedt, for helping us in the initial stages of our work.

Finally, we would like to express our gratitude to the faculty of Electric Power Engineering at Chalmers for their support during the thesis.

Manoj Saladi, Mubashar Bashir,
Gothenburg, June 2019

Nomenclature and Abbreviations

Symbol	Meaning	Unit
L_{sd}	D-axis inductance	H
L_{sq}	Q-axis inductance	H
u_{sd}	D-axis voltage	V
u_{sq}	Q-axis voltage	V
i_{sd}	D-axis current	A
i_{sq}	Q-axis current	A
ψ_{sd}	D-axis flux	Wb
ψ_{sq}	Q-axis flux	Wb
ψ_m	Magnet flux	Wb
n_p	Number of pole-pairs	–
R_s	Stator resistance	Ω
R_d	Diode forward resistance	Ω
R_T	IGBT on-state resistance	Ω
R_{on}	MOSFET on-state resistance	Ω
V_d	Diode forward voltage drop	V
V_T	IGBT on-state voltage drop	V
p_{diode}	Instantaneous diode power loss	W
P_{diode}	Average diode power loss	W
p_{IGBT}	Instantaneous IGBT power loss	W
P_{IGBT}	Average IGBT power loss	W
p_{MOSFET}	Instantaneous MOSFET power loss	W
P_{MOSFET}	Average MOSFET power loss	W
E_{on}	Switch-on energy loss of device	J
E_{off}	Switch-off energy loss of device	J
E_{rec}	Reverse recovery energy of diode	J
m	Modulation Index	–
f_{sw}	Switching frequency	Hz
β	Parallel conduction angle	radians
T_j	Device Junction Temperature	°C

Abbreviations

Abbreviation	Full form
PMSM	Permanent Magnet Synchronous Machine
IPMSM	Interior Permanent Magnet Synchronous Machine
MTPA	Maximum Torque per Ampere
MTPV	Maximum Torque per Volt
HEV	Hybrid Electric Vehicle
PHEV	Plug-in Hybrid Electric Vehicle
IGBT	Insulated Gate Bipolar Transistor
MOSFET	Metal Oxide Semiconductor Field Effect Transistor
PWM	Pulse Width Modulation
Si	Silicon
SiC	Silicon Carbide
AC	Alternating Current
THIPWM	Third Harmonic Injection Pulse Width Modulation
NPV	Net Present Value
LCCA	Life-Cycle Cost Analysis
ECE	European City Manual

Contents

1
Introduction

1.1 Background

In the automotive industry, conventional vehicles are being replaced by hybrid & electric vehicles, and they seem to provide an excellent sustainable solution for future generations[1]. To meet customer requirements, several research works are done, and some are still going on, especially in the improvement of power source (Battery), power conversion unit (inverter) and the electric drive.

The main problem with the electric vehicles is that the energy required for propulsion is provided by batteries or fuel cells whose storage capacity is limited. So the power from the battery has to be utilized wisely at high torque - low speed and low torque - high speed requirements [2] [3].

Apart from the improvements in the electric drive and drive system, a lot of research work also has been going on to identify the benefits of using currently emerging Silicon Carbide MOSFETs instead of commercially being used IGBTs[4][5]. Silicon Carbide MOSFETs have higher blocking voltages and have lower switching losses, so they can be operated at higher switching frequencies when compared to IGBTs.

It can be assured that power taken from the power source is optimal, by implementing a control strategy that includes Maximum Torque per Ampere (MTPA) strategy and Maximum Torque per Volt (MTPV) strategy[6][7]. In such an optimized drive system, analysis of power losses with inverter switches as Silicon Carbide MOSFETs, instead of IGBTs, provide us the information on the power, that can be saved.

1.2 Purpose

The purpose of this thesis is to develop a closed-loop drive system for a non-Linear Permanent Magnet Synchronous Machine with MTPA and MTPV control strategies implemented. For such a drive system, a comparison is made for power losses when Si-based IGBTs and SiC-based MOSFETs are used.

1.3 Problem/Task

Considering a linear machine model makes the drive system construction much easy. However, in the real application, the analysis made on the linear model cannot be used. In a linear model d and q-axis inductances are assumed to be constant, magnetic saturation is neglected. Such assumptions lead to improper control of PMSM. Therefore in this thesis work, a nonlinear PMSM is built in Simulink for the drive system analysis and MTPA and MTPV strategies are implemented in the current reference calculation block, so that the current references produced follow the nonlinear behavior.

The inverter loss analysis is done, for every speed-torque operating point obtained by MTPA & MTPV strategies, by considering the analytical equations mentioned in chapter 2.6. However, to make the comparison simple, the loss comparison is shown for one of the operating points, since the comparison almost remains the same for the rest of the operating points. Third Harmonic Injection Pulse Width Modulation (THIPWM) is implemented to analyze the inverter losses. The common-mode injection method is used for the THIPWM, and the loss comparison is made on a single operating point.

Life-Cycle Cost Analysis (LCCA) model is derived by considering only the initial cost and energy cost involved over the defined lifetime of the power inverters. City Manual part of the New European driving cycle is used for the loss calculation in the inverters, and the Net present Value (NPV) of the losses in terms of money is calculated for considering the inflation and interest rate.

1.4 Scope

A closed loop drive system is built for a non linear PMSM in Matlab/Simulink by considering non linearity as mentioned in purpose. Speed control is not considered in the the drive system, since the focus is to make analysis for all torque speed operating points or a driving cycle.

The drive system built in Simulink is not used for inverter loss analysis, instead analytical equations are used. A simple resistive thermal network is used for thermal feedback in loss evaluation. In the LCCA, operational and disposal costs are ignored for simplicity in the model, and only the City Manual (ECE) part of the New European driving cycle (NEDC) is considered in the loss calculation in inverters.

1.5 Sustainable Aspects and Code of Ethics

The automotive industry has been transforming, and soon, most of today's conventional combustion engine vehicles are going to be replaced with electric and hybrid vehicles, many studies have predicted that there would be around one million Plug-in Electric vehicles (PEVs) [8] . All this transformation is based on one intention, that is to make transportation more sustainable[1]. The present technology in the automotive industry is silicon-based, silicon-based IGBTs are the most commonly

used power electronic switches to convert the DC power from the battery into AC power for the motors, but the IGBTs used nowadays mainly have limitations like maximum allowable operating temperature and switching frequency [9].

To make the technology sustainable, the automotive industry has been looking into silicon carbide-based technology to replace the currently used Si-based IGBTs with SiC-based MOSFETs, since SiC MOSFETs have considerable advantages when compared to IGBTs. By replacing Si with SiC devices, almost 70-80% of switching losses can be reduced [10]. Therefore SiC MOSFET modules can be operated at higher switching frequencies compared to IGBTs; also MOSFET modules occupy less space when compared to IGBT modules because more IGBT modules have to be used to deliver the same output that less number of MOSFET modules can deliver.

However, the problem using SiC MOSFETs is that the technology is relatively new, expensive, and more circuit complexity involved. Moreover, the current status of SiC MOSFETs is that they are only used if and only if one wants to increase the performance. So, SiC devices are still waiting for the breakthrough in the application, since still there is a need for improvement in the quality of these devices [11].

Apart from the focus on sustainable aspects, some IEEE code of ethics has been followed while carrying out this thesis work. The work is done genuinely and claims, estimates, and results shown in this report are realistic.

1.6 Thesis Outline

Thesis work is carried out as chapters layout is being exhibited.

- **C**hapter 2: Theory about different PMSMs, saliency, modelling of power electronic devices, third harmonic injection, life-cycle cost analysis
- **C**hapter 3: Approach to conduct the simulations of PMSM control, three phase inverter loss calculations and model development of life-cycle cost analysis
- **C**hapter 4: Results of control of PMSM, inverter power losses and life cycle cost analysis
- **C**hapter 5: Thesis conclusion and future work

2
Theory

2.1 Permanent Magnet Synchronous Machine

The Permanent magnet synchronous motor (PMSM) is a kind of an AC synchronous machine where the rotor's permanent magnets produce the rotor magnetic flux instead of excitation through rotor windings. The permanent magnet machines are widely used in industrial applications due to their high torque/inertia ratio, high power density, and high efficiency over a wide range of speed and torque [12].

The working of permanent magnet machines is different in comparison with an electrically excited synchronous machine. For a PMSM in the open-loop operation, the uncontrollable rotor flux doesn't let the rotor to catch up with the rotating magnetic field of the stator. Due to this, the rotor keeps oscillating all the time during the operation. So, the permanent magnet machines always require a closed-loop control technique to reduce the stator flux frequency to a sufficiently low value such that rotor magnetic flux can be synchronized with the stator flux.

2.1.1 Types of permanent magnet machines

Permanent magnet synchronous machines can be classified into three types based on the placement of rotor magnets on/in the rotor. As shown in Fig. 2.1(a) if the magnets are mounted on the motor's rotor surface then it is called a surface-mounted PMSM, but if the rotor's magnets buried deep into the rotor construction then it is called interior PMSM as shown in Fig. 2.1(c).

The relative permeability of the magnets $\mu_{r.mag}$ is almost equal to air permeability $\mu_{r.air}$

$$\mu_{r.mag} \approx \mu_{r.air} = 1 \tag{2.1}$$

The machine's rotor core is made of iron or other material which has higher permeability when compared to air $\mu_{r.air}$

$$\mu_{r.core} \gg \mu_{r.air} \tag{2.2}$$

In a surface-mounted PMSM, the magnets placed on the rotor's surface have the same permeability as air due to which there is no saliency in this machine. This relation can be expressed as

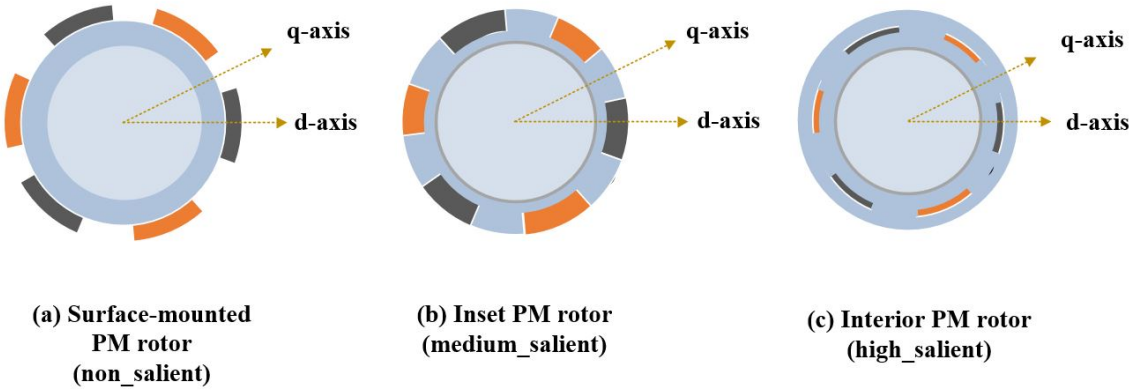

Figure 2.1: Classification of PMSM rotors

$$L_{sd} = L_{sq} \tag{2.3}$$

where L_{sd} is the inductance of the d-axis and L_{sq} is the inductance of the q-axis.

In an IPMSM, the magnets are buried inside the rotor. As there is a magnet in the d-axis direction, its effective permeability is lesser when compared to the permeability in q-axis direction. Because of this the flux easily passes in the q-axis direction than in the d-axis direction. The relation between d and q-axis inductances is given by (2.4)

$$L_{sd} < L_{sq} \tag{2.4}$$

due to the saliency in an IPMSM, an extra torque called Reluctance Torque can be produced, which is a product of d and q-axis currents, in addition to Reactive Torque which is proportional to q-current. More explanation about these torques is mentioned section 2.4.2.

Some advantages of using IPMSM are as follows

- High mechanical strength
- Small magnetic air gap
- Large torque to inertia ration
- High power density &
- High efficiency.

2.2 Coordinate System Transformation

Generally, a drive system is built based on the rotating coordinate system or the d-q coordinate system. It is challenging to build a control system based on three-phase AC quantities, that's why it is more beneficial to convert these three-phase AC quantities into DC quantities which are called direct axis (d-axis) and quadrature

(q-axis) components. Fig. 2.2 shows the stationary $\alpha\beta$-frame, which is transformed into d-q coordinate system.

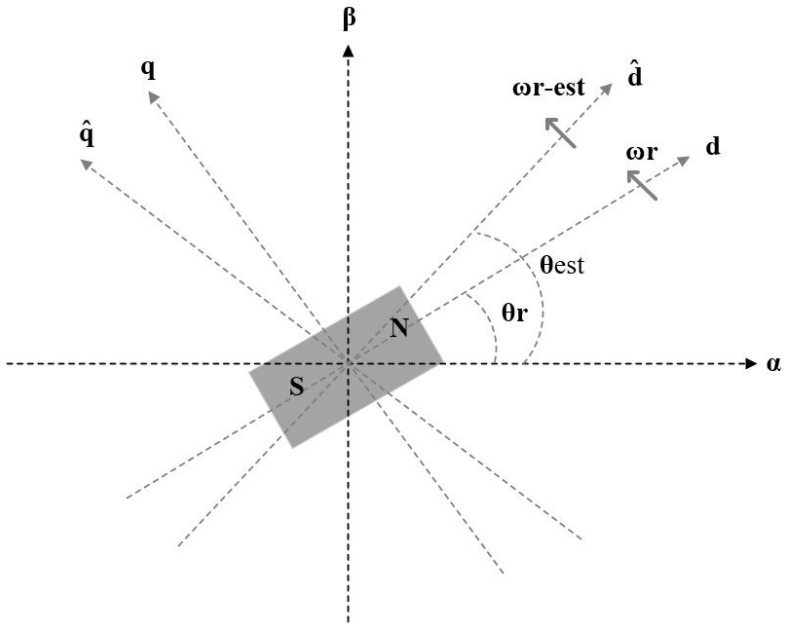

Figure 2.2: Definition of the $\alpha\beta$, dq and $\hat{dq}$ coordinate systems

By using Clarke transformation, first, the three-phase AC quantities can be converted into two-phase AC quantities, called alpha (α) and beta(β) quantities, as

$$\begin{bmatrix} x_\alpha \\ x_\alpha \end{bmatrix} = \begin{bmatrix} \frac{2}{3} & \frac{-1}{3} & \frac{-1}{3} \\ 0 & \frac{1}{\sqrt{3}} & \frac{-1}{\sqrt{3}} \end{bmatrix} \begin{bmatrix} x_\alpha \\ x_\beta \\ x_c \end{bmatrix} \tag{2.5}$$

The α-component is aligned with the x-axis, and the β-component is leading it by 90°, but the dq-coordinate system is a rotating coordinate system with the rotor speed ω_r, as shown in Fig. 2.2. Both the d-axis and q-axis are 90° from each other and rotating anticlockwise. By using Park transformation, rotation can be added to these α, β components as

$$\begin{bmatrix} x_d \\ x_q \end{bmatrix} = \begin{bmatrix} \cos(\theta_r) & \sin(\theta_r) \\ -\sin(\theta_r) & \cos(\theta_r) \end{bmatrix} \begin{bmatrix} x_\alpha \\ x_\beta \end{bmatrix} \tag{2.6}$$

Sensor and sensorless control schemes are used to estimate the rotor position to align the d-axis with the rotor flux, so the rotor flux and angular position of the d-axis is denoted as θ_r. That's why it is essential to estimate the rotor position correctly to have a better control system.

However, in reality, It is not possible to estimate the rotor position precisely due to different factors like the rotor design and edge effect. Accordingly, the estimated dq-frame is denoted as

$$\theta_{est} = \theta_r - \hat{\theta}_r \tag{2.7}$$

The transformation from the real dq-frame to the estimated dq-frame can be done as

$$\begin{bmatrix} x_d \\ x_q \end{bmatrix} = \begin{bmatrix} \cos(\theta_e) & \sin(\theta_e) \\ -\sin(\theta_e) & \cos(\theta_e) \end{bmatrix} \begin{bmatrix} \hat{x_d} \\ \hat{x_q} \end{bmatrix} \tag{2.8}$$

2.3 Linear Vs Nonlinear PMSM Model

In a linear model, L_{sd} and L_{sq} are assumed to be constant under any operating condition, and there is no combined relationship between d and q-axis currents, i_{sd} & i_{sq}, with d and q-axis fluxes, ψ_{sd} & ψ_{sq}. That is why ψ_{sd} is only dependent on i_{sd} & ψ_{sq} is only dependent on i_{sq}. Therefore the voltage equations of such a linear model model can be written as

$$u_{sd} = R_s i_{sd} + L_{sd}\frac{di_{sd}}{dt} - \omega_r L_{sq} i_{sq} \tag{2.9}$$

$$u_{sq} = R_s i_{sq} + L_{sq}\frac{di_{sq}}{dt} + \omega_r L_{sd} i_{sd} + \omega_r \psi_m \tag{2.10}$$

Where R_s is stator resistance , ψ_m is the magnet flux and ω_r is electrical speed of the motor.

The difference between linear and non-linear model can be well understood by comparing dependencies of the fluxes on the currents. The stator flux equation of the linear model can be written as

$$\psi_s = L_{sd} i_{sd} + \psi_m + j L_{sq} i_{sq} \tag{2.11}$$

upon splitting, (2.11) into its real and imaginary parts, d and q-axis fluxes can be written as

$$\psi_{sd} = L_{sd} i_{sd} + \psi_m \tag{2.12}$$

$$\psi_{sq} = L_{sq} i_{sq} \tag{2.13}$$

and from (2.12) and (2.13) it is clear that ψ_{sd} is only dependent on i_{sd} and ψ_{sq} is only dependent on i_{sq} when considering L_{sd}, L_{sq} and ψ_m as constants. However, (2.12) and (2.13) are not valid in the case of a non-linear model, since ψ_{sd} and ψ_{sq} are both the functions of i_{sd} and i_{sq} as well as the terms L_{sd}, L_{sq} and ψ_m are also variable. Generally the interference of i_{sq} with ψ_{sd} is more when compared to the interference of i_{sd} with ψ_{sq}.

2.4 Torque Control of PMSM

In this section, explanations about the IPMSM torque equation, reactive torque and reluctance torque, voltage and current constraints, MTPA & MTPV strategies are provided. The principle of torque production in an IPMSM is not as simple as in other PMSM configurations, so it would be good to know some background information before proceeding into motor control.

2.4.1 Derivation of PMSM torque equation

The electrical input power to a 3-phase electrical machine can be expressed as

$$P_{abc}(t) = u_a(t)i_a(t) + u_b(t)i_b(t) + u_c(t)i_c(t) \tag{2.14}$$

here, u_a, u_b & u_c are the phase voltages, i_a, i_b & i_c are the phase currents. This three phase instantaneous power in $\alpha\beta$ coordinate system can be written as

$$P_{\alpha\beta}(t) = \frac{3}{2K^2}\Big(u_\alpha(t)i_\alpha(t) + u_\beta(t)i_\beta(t)\Big) = \frac{3}{2K^2}Re\{u_s^s i_s^{s*}\} \tag{2.15}$$

by adding rotation to vectors, $u_s^s = u_s e^{j\theta_r}$ and $i_s^s = i_s e^{j\theta_r}$. Eq (2.15) in dq coordinate system can be expressed as

$$P_e = \frac{3}{2K^2}Re\{u_s i_s^*\} = \frac{3}{2K^2}Re\{j\omega_r \psi_s i_s^*\} \tag{2.16}$$

For a complex number Re{jz}=-Im{z}, therefore (2.17) becomes

$$P_e = -\frac{3\omega_r}{2K^2}Im\{\psi_s i_s^*\} = \frac{3\omega_r}{2K^2}Im\{\psi_s^* i_s\}, \tag{2.17}$$

since stator flux is given by 2.11, and by assuming amplitude invariant transformation Eq.2.17 can be written as

$$P_e = \frac{3\omega_r}{2}\Big((L_{sd} - L_{sq})i_{sd}i_{sq} + \psi_m i_{sq}\Big) \tag{2.18}$$

Electro-mechanical torque can be expressed as

$$T_e = \frac{P_e}{\Omega_r} \tag{2.19}$$

Ω_r is the mechanical speed and is expressed as $\Omega_r = \omega_r/n_p$ so

$$T_e = \frac{n_p P_e}{\omega_r} \tag{2.20}$$

By substituting (2.18) in (2.20), finally the torque equation of a PMSM can be written as

$$T_e = \frac{3n_p}{2}\Big(\psi_m i_{sq} + (L_{sd} - L_{sq})i_{sq}i_{sd}\Big) \tag{2.21}$$

2.4.2 Reactive torque and Reluctance torque

The motor in a HEV or in Plug-in Hybrid Electric Vehicles (PHEV) should be able to provide high torque during the low speed and operate in constant power region. It is known that the electromagnetic torque of the motor is proportional to the current supplied to it. Therefore due to the high current requirements at start-up, the current should be optimal to reduce the copper losses associated with it.

In a non-salient permanent magnet machine, the stator current and the rotor magnetic field should be orthogonal to each other to obtain the maximum torque. However, in the IPMSM, the angle between the stator current and the rotor magnetic field is not always orthogonal due to saliency and changes with the required current magnitude to produce the corresponding torque.

For lower current magnitudes the functionality of the IPMSM is similar to the PMSM, whereas at high current magnitudes it is similar to a synchronous reluctance machine. The first term of (2.21) corresponds to the field/reactive torque, whereas the second term corresponds to the reluctance torque, which is due to the product of i_{sq} and i_{sq}. It is known that due to saliency L_{sd} is less than L_{sq}, and if i_{sd} is negative, it results in an addition of the reluctance torque which finally increases the total torque.

Due to the change of functionality of the IPMSM depending upon the current magnitude, the angle between the stator current and the rotor flux is no longer 90 degrees. This angle is also called the control angle (β). For example, under the high current magnitude scenario if the MTPA technique is disregarded, then the major part of the current may be on the q-axis, which results in loss of the reluctance torque. On the dq-plane, there would be many i_{sd} and i_{sq} combinations that produce the same torque. Among these pairs, there is only one optimum i_{sd} and i_{sq} and is generally closer to the origin. This pair can be obtained if the MTPA technique is considered.

2.4.3 Voltage and current constraints

In a PMSM, in a drive system, the maximum current limit is the rated current of the motor, and the maximum voltage limit is the output voltage of the inverter. As the drive system is built based on dq - axis model, the current and voltage limit equations are given as

$$\sqrt{{i_{sd}}^2 + {i_{sq}}^2} = I_s \leq I_{max} \tag{2.22}$$

$$\sqrt{{u_{sd}}^2 + {u_{sq}}^2} = U_s \leq U_{max} \tag{2.23}$$

where U_s & I_s are the magnitudes of stator voltage and stator current. U_{max}, I_{max} are maximum limits of stator voltage and stator current respectively. By neglecting the ohmic voltage drop and considering steady state, (2.9) and (2.10) can be rewritten as

$$u_{sd} = -\omega_r L_{sq} i_{sq} \tag{2.24}$$

$$u_{sq} = \omega_r L_{sd} i_{sd} + \omega_r \psi_m \tag{2.25}$$

By substituting (2.24) & (2.25) in (2.23) the voltage limit equation is obtained

$$\frac{(i_{sd} + \frac{\psi_m}{L_{sd}})^2}{\frac{U_s^2}{\omega_r^2 L_{sd}^2}} + \frac{(i_{sq})^2}{\frac{U_s^2}{\omega_r^2 L_{sq}^2}} = 1 \tag{2.26}$$

The voltage and current limit equations are useful in understanding MTPA and MTPV strategies, which are explained in the following section.

2.4.4 Optimal operation of an IPMSM

An IPMSM can be operated efficiently by implementing MTPA and MTPV strategies. These strategies are explained using (2.22) & (2.26) which represents current limit and voltage limit equations respectively. Eq.(2.22) represents a circle with radius I_{max} and (2.26) is in the form of an ellipse whose center is $(\frac{-\psi_m}{L_{sd}}, 0)$, and indicates that the stator flux limit is inversely proportional to the rotor speed.

Fig. 2.3 shows the characteristic curves of an IPMSM. The ellipses are limits for the flux at speeds ω_a, ω_b, ω_c where $\omega_a < \omega_b < \omega_c$, the size of the flux ellipse shrinks as the rotor speed increases. For speeds, less than ω_a the stator flux limit ellipse is sufficiently large such the maximum torque T_4 is only limited by the maximum current, which is indicated as point A. Therefore for the speeds less than ω_a, the optimum current path follows the red curve, which is the so-called 'Maximum Torque per Ampere' curve. The intersection of the torque (blue dashed hyperbolas) and the MTPA curve represents the most optimal pair of the current references to produce the specific torque inside the voltage and current limit.

When the speed is higher than ω_a, the optimum current strategy is no longer valid, because now the operation of the motor is limited by the stator flux alongside with the maximum inverter current. Consider now, that ω_b is the rotor speed, so if the

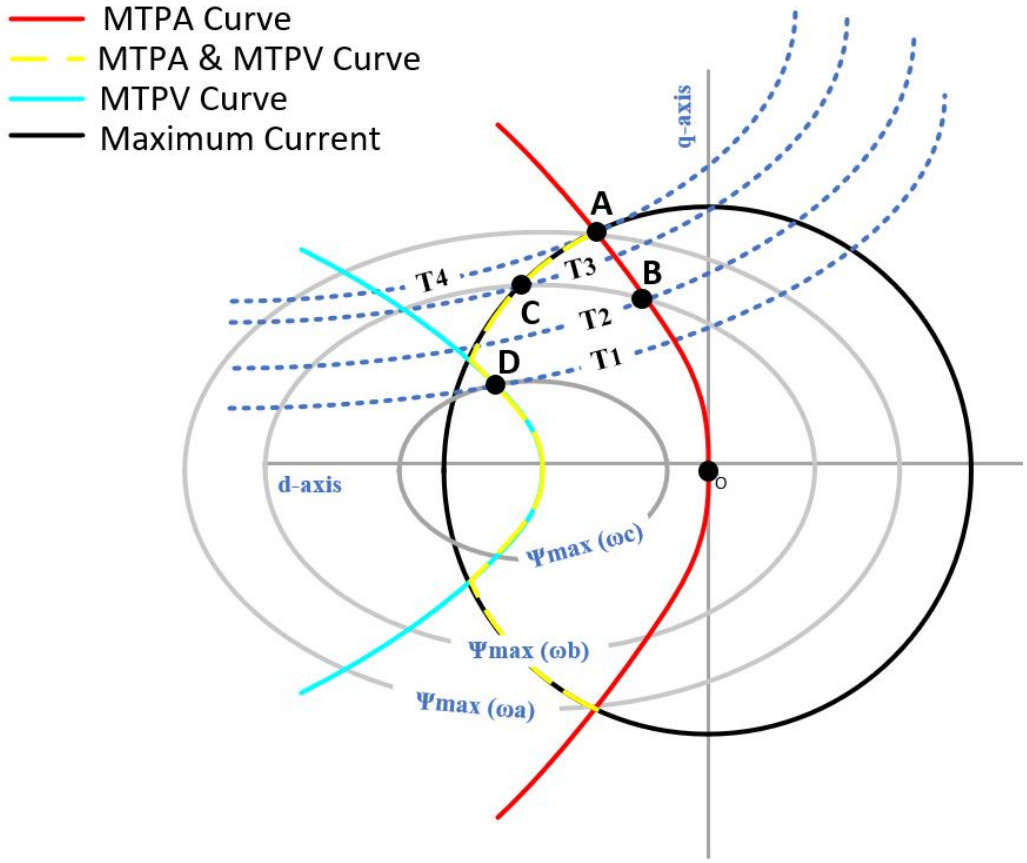

Figure 2.3: Stator current based characteristic curves of an IPMSM

motor speed is beyond this, the induced voltage crosses the allowed limit. The available torques at this speed are T_1,T_2 and T_3, where T_1, T_2 can be produced simply with the optimum current following the MTPA path, but to produce torque T_3 the MTPA path can no longer be followed because of the flux constraint. So, to produce produce T_3 torque, more negative i_{sd} has to be supplied to the motor than what it is supposed to be given to extract the achievable reluctance torque, this process is called partial field weakening, and the operating point shifts from point B to Point C.

If the center of the concentric ellipses lies inside of the motor's maximum current limit, then the short circuit current of the motor is less the maximum current. Such motors are theoretically named as infinite speed drives, where there is no electrical limitation at higher rotor speeds. The only constraint for the rotor speed is voltage limit, and the operating point is now shifted to point D and moves along the yellow dashed line and approaches center as rotor speed increases towards infinity. The locus of the operating point is now called the Maximum Torque Per Volt curve, and this process is called full-field weakening.

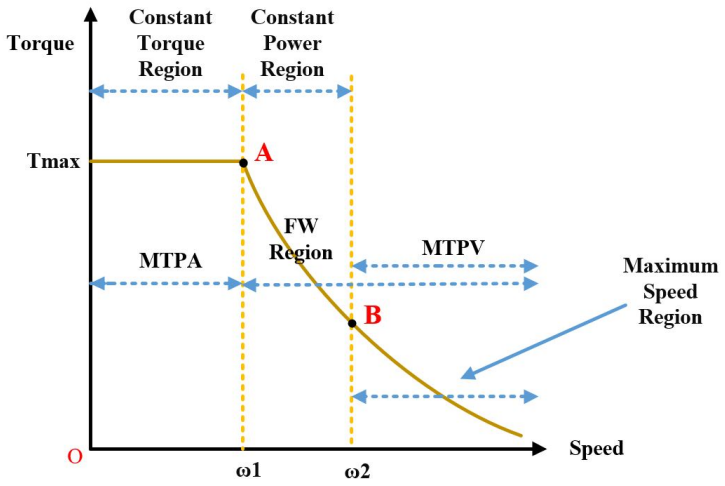

Figure 2.4: Torque vs speed characteristics

Fig. 2.4 shows torque-speed characteristics plot, it represents constant torque region and how the torque demand has to be reduced at high speeds in the constant power region or partial and full-field weakening regions.

2.5 Power Semiconductor Devices

In this section, the working principles of different power semiconductor devices, used in inverters, are explained. As in this thesis work, power loss comparison is made between IGBT/SiC MOSFET inverters; it is necessary to have a glance at the working principles of IGBTs, MOSFETs & Diodes.

2.5.1 Working principles of Diode, IGBT & MOSFET

The working of different power semiconductor devices can be explained by modeling them in terms of their electrical equivalent circuits by looking at their current-voltage or i-v characteristics, from which also the power loss equations can be derived later. The diode symbol and its i-v characteristics are shown in the Fig. 2.5

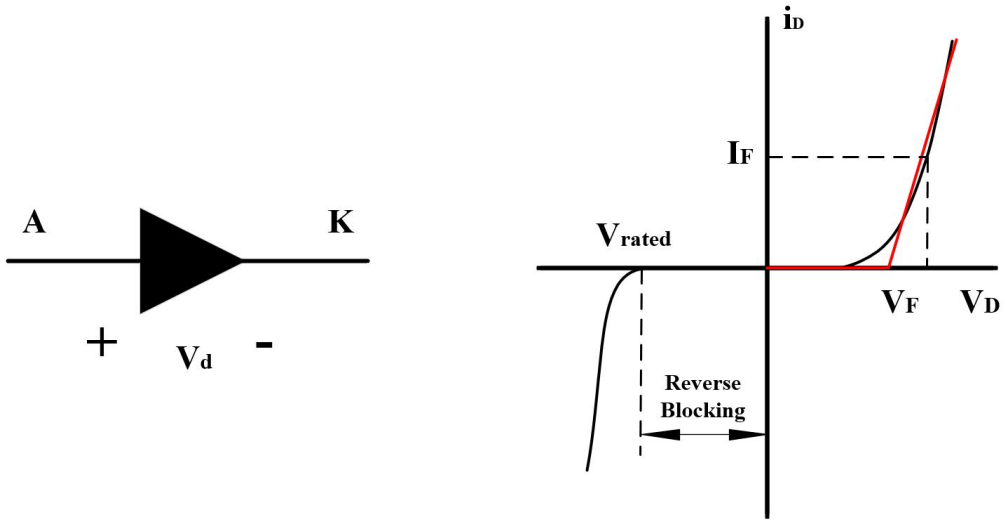

Figure 2.5: Symbol,iv - Characteristics of diode

To derive the equivalent circuit, approximating the forward characteristics as the red line in the figure simplifies the diode parameter calculation. The distance from the origin to the intersection point of the red line with the x-axis is the forward voltage drop V_d and the slope of the red line gives the diode forward resistance R_d. Therefore a diode can be modeled as a resistance in series with a voltage source, as shown in the Fig. 2.6

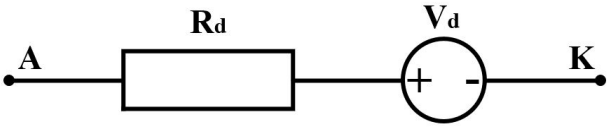

Figure 2.6: Equivalent circuit of diode

From the equivalent circuit above, the power loss equations can be derived as

$$p_{diode}(t) = (R_d i(t) + V_d) i(t) = R_d i^2(t) + V_d i(t) \tag{2.27}$$

$$\begin{aligned} P_{diode}(t) &= \frac{1}{T} \int_0^T (R_d i(t) + V_d) i(t) dt \\ &= \frac{1}{T} \int_0^T (R_d i^2(t) + V_d i(t)) dt \\ &= R_d i_{rms}^2 + V_d i_{avg} \end{aligned} \tag{2.28}$$

where p_{diode} is the instantaneous power loss and P_{diode} is the average power loss, i_{rms} is the RMS current and i_{avg} is the average current and T is the time period.

An Insulated Gate Bipolar Transistor (IGBT) is a Bipolar Junction Transistor with an insulated gate; it has three terminals, namely Gate, Collector, and Emitter. The output characteristics of IGBT are similar to forward characteristics of the diode, except the thing that the characteristic curves saturate at different levels based on the Gate to Emitter voltage level V_{GE}, as shown in the Fig. 2.7. Therefore the equivalent circuit model of an IGBT is similar to the diode equivalent circuit as shown in Fig. 2.8.

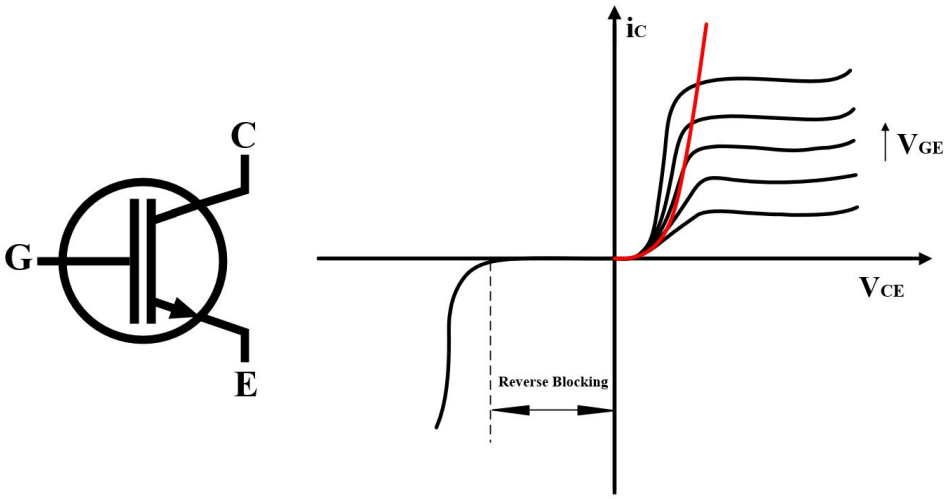

Figure 2.7: Symbol, iv - characteristics of IGBT

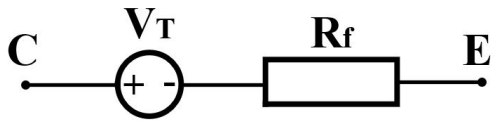

Figure 2.8: Equivalent circuit of IGBT

The on-state power loss equations of IGBT can be written as

$$p_{IGBT} = (R_f i(t) + V_T) i(t) = R_f i(t)^2 + V_T i(t) \tag{2.29}$$

$$\begin{aligned} P_{IGBT}(t) &= \frac{1}{T} \int_0^T (R_f i(t) + V_T) i(t) dt \\ &= \frac{1}{T} \int_0^T (R_f i^2(t) + V_T i(t)) dt \\ &= R_f i_{rms}^2 + V_T i_{avg} \end{aligned} \tag{2.30}$$

The Metal-oxide Semiconductor field-effect Transistor (MOSFET) is also a three-terminal device MOSFET named as Gate, Source and Drain. Unlike diode and IGBT, MOSFETs don't have a forward voltage drop. The symbol and i-v characteristics of an N - channel MOSFET is shown in the Fig. 2.9. It can be observed from the characteristics that MOSFET doesn't have a forward voltage drop, therefore can be modeled only as a resistor R_{on} as shown in the Fig. 2.10

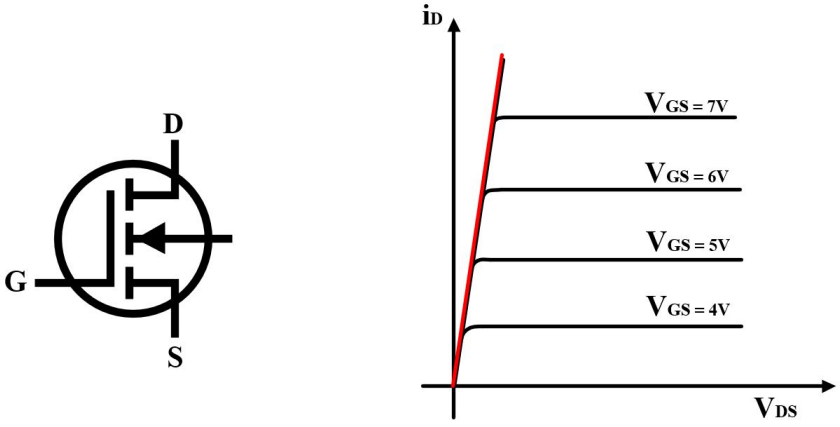

Figure 2.9: Symbol, iv - characteristics of an N - channel MOSFET

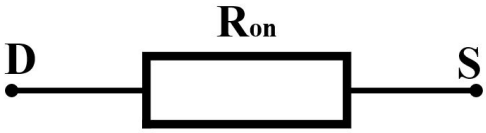

Figure 2.10: Equivalent circuit diagram of a MOSFET

The on-state power loss equations of MOSFET can be derived as

$$p_{MOSFET}(t) = R_{on} i^2(t) \tag{2.31}$$

$$\begin{aligned} P_{MOSFET}(t) &= \frac{1}{T} \int_0^T (R_{on} i^2(t) dt \\ &= R_{on} i_{rms}^2 \end{aligned} \tag{2.32}$$

2.5.2 Silicon Vs Silicon Carbide devices

Si-based IGBTs have been widely used in power electronics, automotive & power system applications since they can be operated at the high switching frequency and the gate circuit complexity is also less. However, Silicon-based technology is saturated in terms of high temperature and high power handling capability, though its an advanced technology. Therefore, the demand has been growing to adapt to Silicon carbide devices, which helps to overcome these problems. SiC devices can block higher voltage levels and can be operated at higher frequencies and higher junction temperatures; they have large bandgap and high critical breakdown field strengths. Also, by using SiC devices, the weight and size of the power converters can be reduced substantially[13][14].

To combine the advantages of higher switching and blocking voltage capabilities, the idea is to use SiC MOSFETs instead of Si IGBTs in power applications. However, SiC MOSFETs have their drawbacks, which surpasses their advantages a little encouraging the usage of Si IGBTs for many applications still. To make the MOSFET suitable for high voltage applications, it is essential to reduce the doping concentration of drift region which increases its resistance and makes it dominating compared to other resistances in the device like channel resistance and accumulation resistance, etc. This relatively high resistance even becomes more at high temperatures, which increases the conduction power losses substantially at higher current magnitudes, wherein Si IGBTs this isn't much a problem because of the lower collector to emitter resistance.

In this thesis work, it is observed that for SiC MOSFETs, the conduction power losses are increasing rapidly with an increase in junction temperature. Whereas for Si IGBTs, the conduction power losses increment isn't that rapid compared to SiC MOSFETs.

2.5.3 Power loss calculation using THIPWM in semiconductor devices

The simple sinusoidal PWM is a straightforward modulation scheme to comprehend, but it doesn't fully utilize the available DC supply voltage[15]. Therefore, Third Harmonic Injection PWM (THIPWM) is implemented to increase the output voltage limit of the inverter for better utilization of the DC-link voltage with minimum harmonic distortion in the output voltage and current. The THIPWM can increase the output voltage by 15.5 percent as compared to the sinusoidal PWM technique. The third harmonic signal is injected into the three-phase reference voltages as shown in Fig. 2.11.

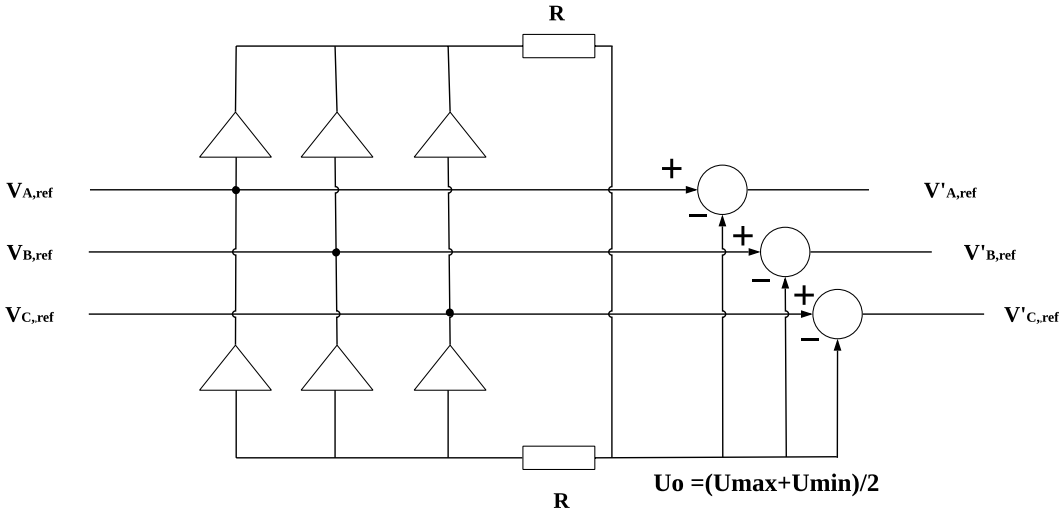

Figure 2.11: Third harmonic injection into the three-phase sinusoidal reference voltages

2.6 Life-Cycle Cost Analysis for the Inverter in the PMSM Drive System

The life-cycle cost analysis (LCCA) of a product or system refers to the total cost associated with the product or system over its defined lifetime[16], and is given by

$$LCCA = purchasingcosts + operatingcosts + maintenancecosts + disposalcosts \tag{2.33}$$

the LCCA technique serves as a useful tool for engineering and economic analyses, especially if a company is looking forward to invest money in capital-intensive,

advanced and emerging technologies[17]. The LCCA analysis can be a primary platform for assessing the economic performance of the suggested assets such as equipment and production systems.

The LCCA model can be useful for the equipment and production system selection process[16]. These characteristics make the LCCA model more suitable for the selection criterion. The LCCA model can assist in the modification in existing systems or equipment, or encourage to invest in modern and efficient technologies. It can also serve as a selection tool between different vendors for purchasing equipment[17].

3
Method

This thesis work aims to find power losses of a three-phase inverter in a permanent magnet synchronous motor drive system. In this work, a lookup table based PMSM model is made to include the non-linearity of the machine in the analysis. Later, a control system is built for this machine model in Matlab/Simulink, as shown in Fig. 4.1, and concepts of MTPA and MTPV are introduced in the torque control and derivation of the d and q-axis current references. The performance evaluation of this drive system is done by giving it with different torque reference values and speed input, as a ramp signal.

3.1 Modeling of the PMSM Drive System

The following sections comprise the explanations of procedure for the development of a field-oriented control system of non-linear PMSM and algorithms for implementation of MTPA & MTPV in the drive system model.

3.1.1 Modeling of PMSM machine

A non linear model of a permanent magnet synchronous machine is shown in the Figs. 3.3 and 3.4. As mentioned in Section 2.3, ψ_{sd} & ψ_{sq} are non linearly dependent on both i_{sd} & i_{sq} . So two dimensional lookup tables or matrices for both ψ_{sd} & ψ_{sq}, as shown in Figs. 3.1 and 3.2, are used in the machine model, since for every i_{sd} and i_{sq} there exists a unique ψ_{sd} and ψ_{sq}.

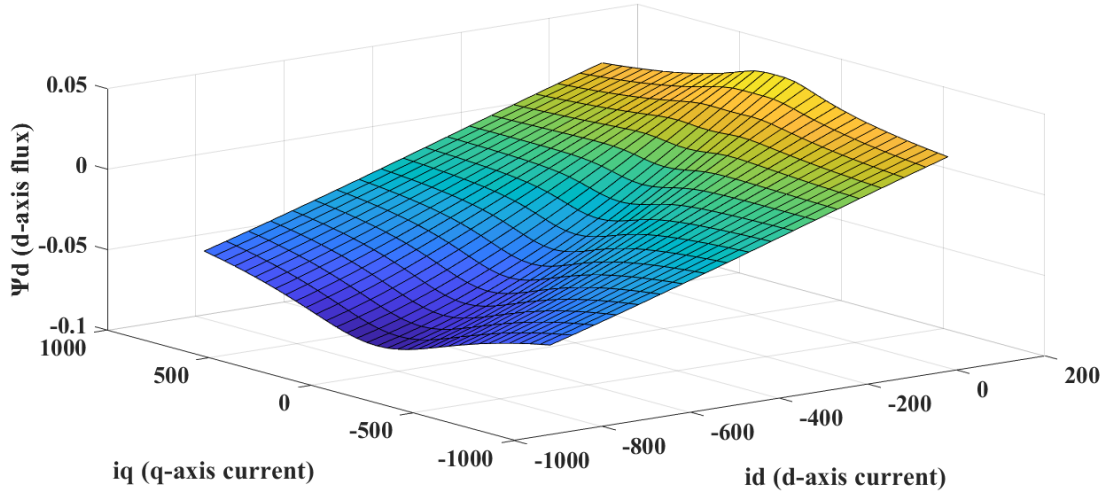

Figure 3.1: Ψ_{sd} (d-axis flux) map

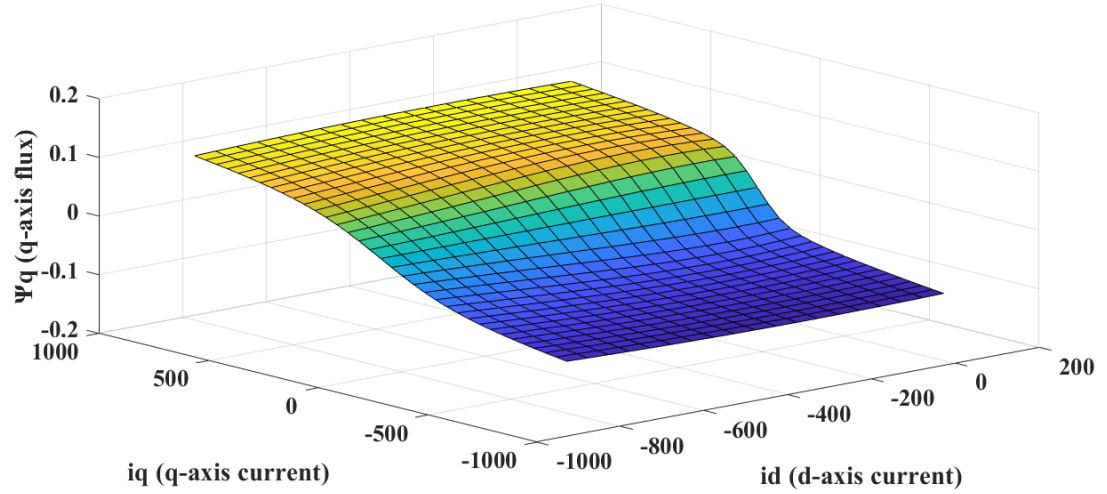

Figure 3.2: Ψ_{sq} (q-axis flux) map

The three phase currents of the PMSM are converted into d-axis and q-axis currents and fed to ψ_{sd} & ψ_{sq} lookup tables to derive the ψ_{sd} & ψ_{sq} for corresponding i_{sd} & i_{sq} values. By measuring three phase currents and speed of the machine, the rate of change of ψ_{sd} & ψ_{sq} are obtained by using (3.1) & (3.2)

$$\frac{d\psi_{sd}}{dt} = u_{sd} - R_s i_{sd} + \omega_r \psi_{sq} \tag{3.1}$$

$$\frac{d\psi_{sq}}{dt} = u_{sq} - R_s i_{sq} - \omega_r \psi_{sd} \tag{3.2}$$

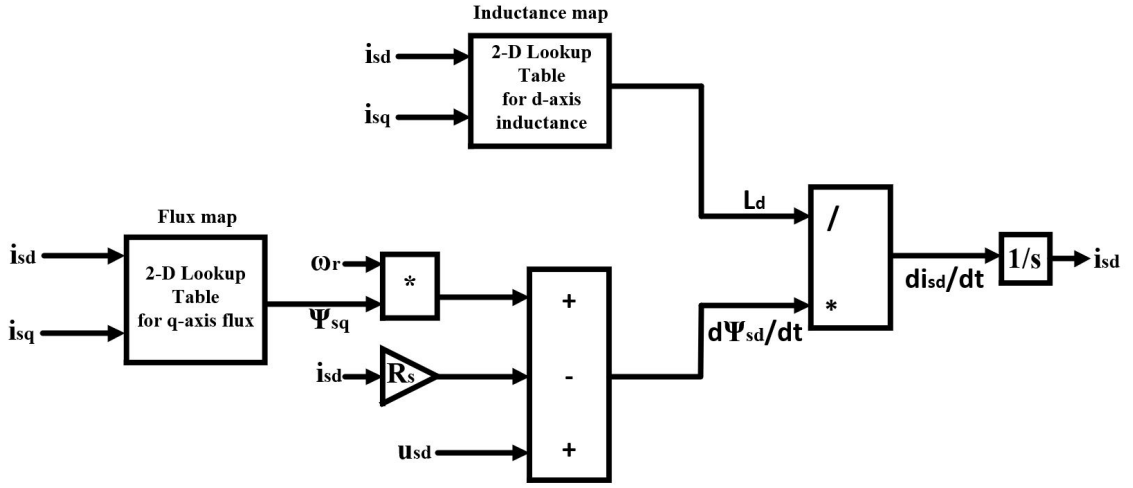

Figure 3.3: Deriving d-axis current

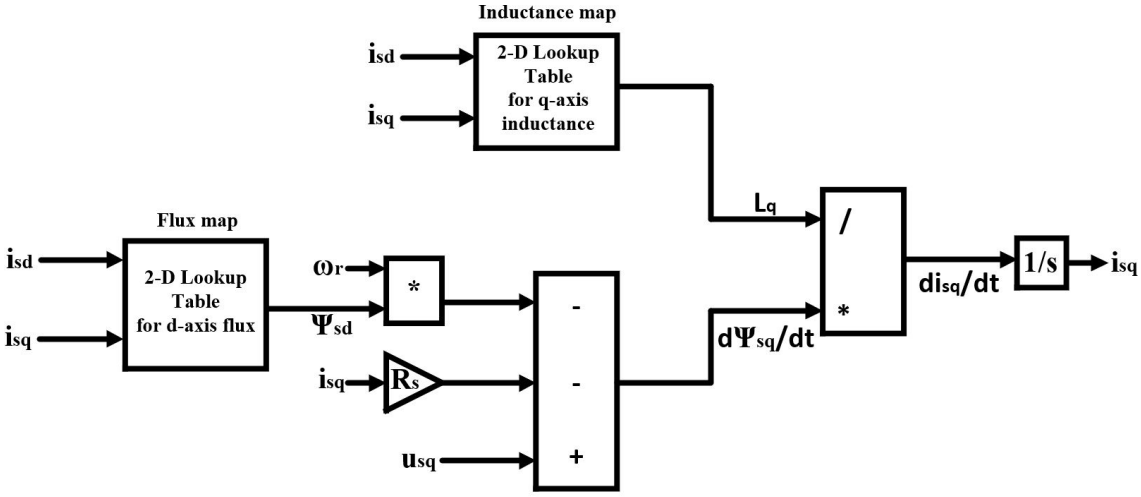

Figure 3.4: Deriving q-axis current

where u_{sd} and u_{sq} are d and q-axis voltages and ω_r is the electrical speed of the machine. In order to obtain i_{sd} & i_{sq}, the rate of change ψ_{sd} and ψ_{sq} have to to be divided with d and q axis incremental inductances and finally integrated, as in (3.3 - 3.6)

$$\frac{\frac{d\psi_{sd}}{dt}}{L_d} = \frac{di_{sd}}{dt} \tag{3.3}$$

$$\int \frac{di_{sd}}{dt} = i_{sd} \tag{3.4}$$

$$\frac{\frac{d\psi_{sq}}{dt}}{L_q} = \frac{di_{sq}}{dt} \tag{3.5}$$

$$\int \frac{di_{sq}}{dt} = i_{sq} \tag{3.6}$$

The electromagnetic torque of the PMSM is obtained as shown in the Fig. 3.5.

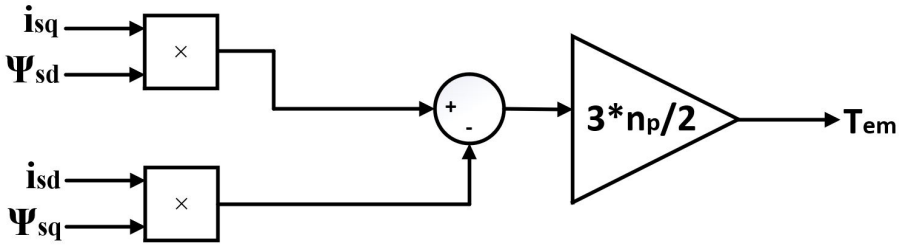

Figure 3.5: Tem calculation

3.1.2 Modeling of current reference calculation block

The purpose of the current reference calculation block is that it calculates the reference values of i_{sd} and i_{sq} for corresponding torque reference and speed input, it contains matrices for i_{sd}, i_{sq}, ψ_{sd}, ψ_{sq}, torque & speed those which are obtained by implementing MTPA and MTPV algorithms using the flux maps mentioned in section 3.1.1.

The ratings of the machine are given in Table 3.1. The algorithm to derive the reference calculation block can be explained as follows. At first a vector for electrical speed of the machine is created which ranges from zero to maximum speed of the machine. Then for every speed value corresponding u_{sd}, u_{sq} & and voltage amplitude are derived using (3.1), (3.2) & (2.23) respectively, in these equations ω_r is a scalar whereas i_{sd}, i_{sq}, ψ_{sd} & ψ_{sq} are matrices. Therefore for every speed, u_{sd}, u_{sq} and voltage amplitude obtained are matrices.

Table 3.1: PMSM Ratings

Parameters	Value	Unit
DC Link voltage	300	V
Rated current	430 RMS	A
Pole Pairs	4	
Maximum speed	11000	RPM

During the first iteration that is during the first speed value, after calculating u_{sd}, u_{sq} & and voltage amplitude, a logical statement is written to filter out the values of i_{sd}, i_{sq}, ψ_{sd}, ψ_{sq} & T_{em} which lie outside of U_{max} and I_{max}, while keeping all the

values which lie within the ratings. Among the kept values of T_{em}, there is only one maximum value. Now the maximum values of i_{sd}, i_{sq}, ψ_{sd}, ψ_{sq} corresponding to this maximum T_{em} value, lie in a position whose index number is same as the index number of maximum value of T_{em}. In this way maximum values of i_{sd}, i_{sq}, ψ_{sd}, ψ_{sq} can be obtained and stored into variables during every iteration. After these iterations, the plot of speed vs. torque is as shown in the Fig. 3.6.

It can be seen in the figure that the obtained values of speed vs. torque are at full torque demand, also the values of i_{sd}, i_{sq}, ψ_{sd} and ψ_{sq}. However, the vehicle might not start every time with full torque demand. Therefore the values of i_{sd}, i_{sq}, ψ_{sd} and ψ_{sq} are required for any percentage value of the torque demand. Therefore a vector is created which consists of linearly spaced torque values from zero to 90% of the maximum value of the machine torque. Now for every percentage value of the torque, a for loop is made as discussed in the previous paragraph. After this process finally the matrices for torque, i_{sd}, i_{sq}, ψ_{sd} & ψ_{sq} can be obtained, whereas speed matrix is obtained by representing the speed vector, mentioned before, in the form of a matrix. The obtained speed vs torque points & i_{sd} vs i_{sq} are shown in the Fig. 3.7 & Fig. 3.8

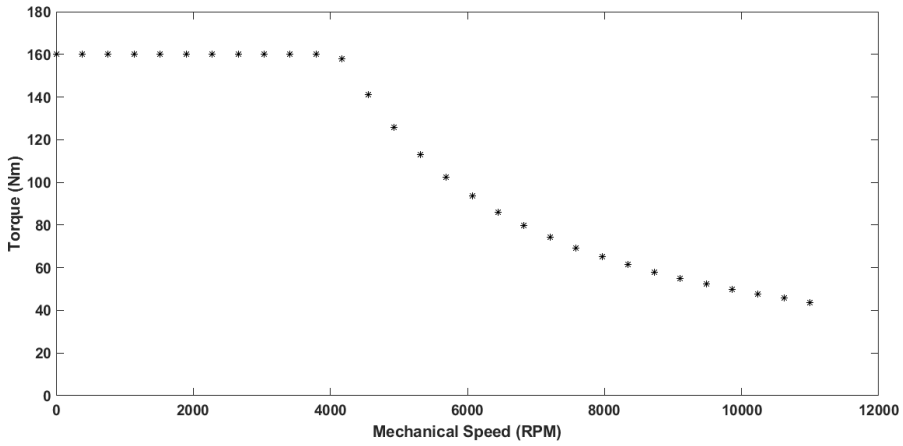

Figure 3.6: Speed vs torque at full torque demand

The i_{sd}, i_{sq}, ψ_{sd} and ψ_{sq} matrices thus obtained can be interpolated using MMatlab interpolation functions. For this purpose, Matlab function is used in the Simulink, which consists of a function that finds the $i_{sd,ref}$ & $i_{sq,ref}$ for the corresponding speed and torque inputs/references. The block diagram of the current reference calculation block is as shown in Fig. 3.9.

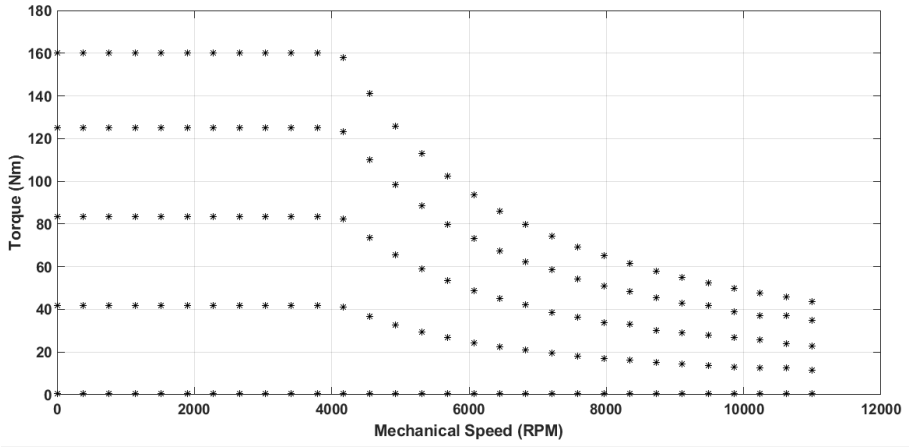

Figure 3.7: Speed vs torque

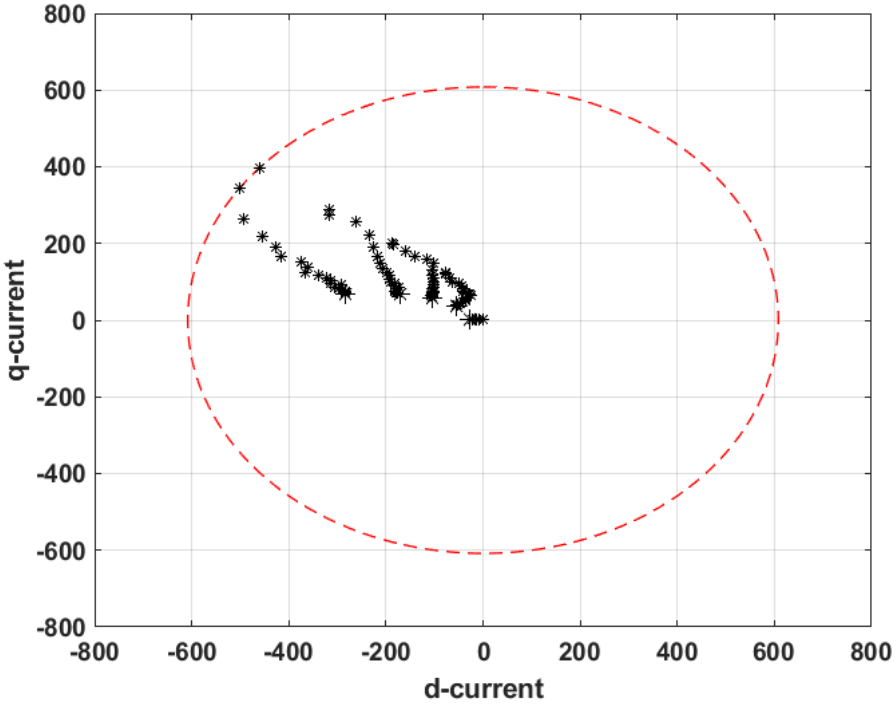

Figure 3.8: i_{sd} vs i_{sd}

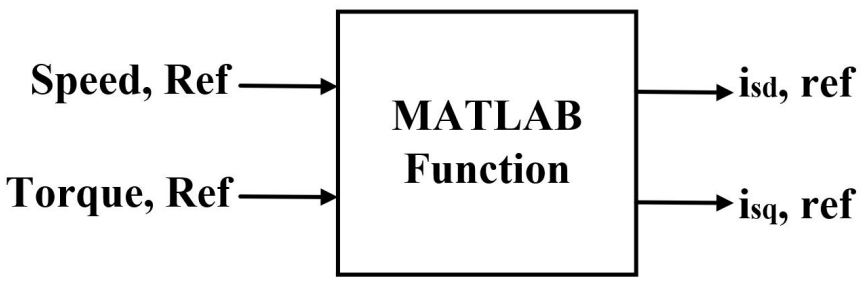

Figure 3.9: Current reference calculation block

3.1.3 Modeling of current controller

A current controller is a block which converts the current references into their corresponding voltage signals. A proportional-Integral controller is used in this work. The complete block diagram of the current controller is as shown in Fig. 3.10. The modelling of the current controller is based on (3.1) & (3.2). The terms $\omega_r\psi_{sq}$ in (3.1) and $\omega_r\psi_{sd}$ in (3.2) are the cross coupling terms which make the equations dependent on one another, $\omega_r\psi_{sq}$ is negative in (3.1) and $\omega_r\psi_{sd}$ is positive in (3.2) therefore $\omega_r\psi_{sq}$ is added and $\omega_r\psi_{sd}$ is subtracted to the corresponding voltage signals, before they are fed to the PMSM block. This removes the affect of cross-coupling in the outputs.

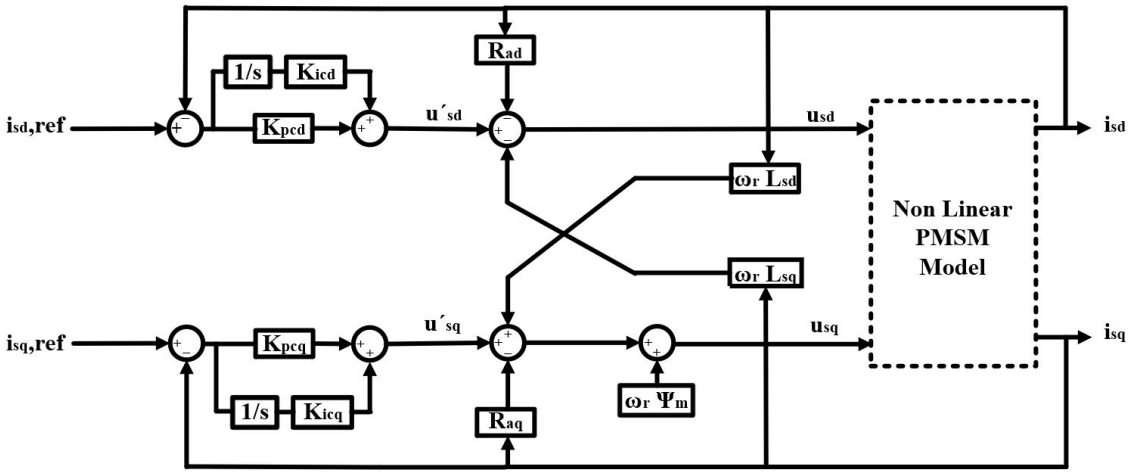

Figure 3.10: Current controller

The term $\omega_r\psi_m$ in (3.2) represents back EMF which is a disturbance, so a feed-forward term of the back EMF is added to the voltage signal, which nullifies the effect of back EMF. In the PI controller, K_{pcd}, K_{pcq}, K_{icd} & K_{icq} are the proportional and integral constants of the d and q-axis respectively. They are derived by considering the closed-loop control system as a first-order low pass filter. Also, an assumption is made that the equations used are linear when deriving these parameters, i.e., unsaturated values of inductances are considered in the calculation of the parameters. K_{pcd}, K_{pcq}, K_{icd} & K_{icq} are given by

$$K_{pcd} = \alpha_c L_{sd} \tag{3.7}$$

$$K_{pcq} = \alpha_c L_{sq} \tag{3.8}$$

$$K_{icd} = \alpha_c (R_s + R_{ad}) \tag{3.9}$$

$$K_{icq} = \alpha_c (R_s + R_{aq}) \tag{3.10}$$

where α_c is the bandwidth of the current current controller which is assumed as 1000 rad/s, R_{ad} & R_{aq} are the active damping resistances and are given by

$$R_{ad} = \alpha_c L_{sd} - R_s \tag{3.11}$$

$$R_{aq} = \alpha_c L_{sq} - R_s \tag{3.12}$$

3.2 Operation Principle of Three Phase IGBT and MOSFET Inverters with Sinusoidal PWM

In this section, the working principles of three-phase IGBT and MOSFET inverters with sinusoidal PWM are explained.

3.2.1 Three-phase IGBT inverter with sinusoidal PWM

When a sinusoidal PWM technique is used in three-phase inverters, the sinusoidal control voltage signal is compared with a triangular carrier wave to produce a pulse width modulated phase voltage signal u_m. To produce u_m, the three-phase sinusoidal voltage signals obtained from the current controller are compared with a triangular wave such that when the sinusoidal is above the triangular wave, then the magnitude of the phase voltage, is $V_{dc}/2$, if not then the magnitude is $-V_{dc}/2$. The polarity of the obtained u_m, along with the polarity of the sinusoidal phase current i_{ph} determines which switches that need to be turned on and off. Here the frequency of the sinusoidal voltage signal is dependent on the angular electric speed of the machine, whereas the frequency of the triangular wave is the frequency of the switching. By implementing the above discussed PWM technique, the phase voltage and the phase current would be as shown in Fig. 3.11

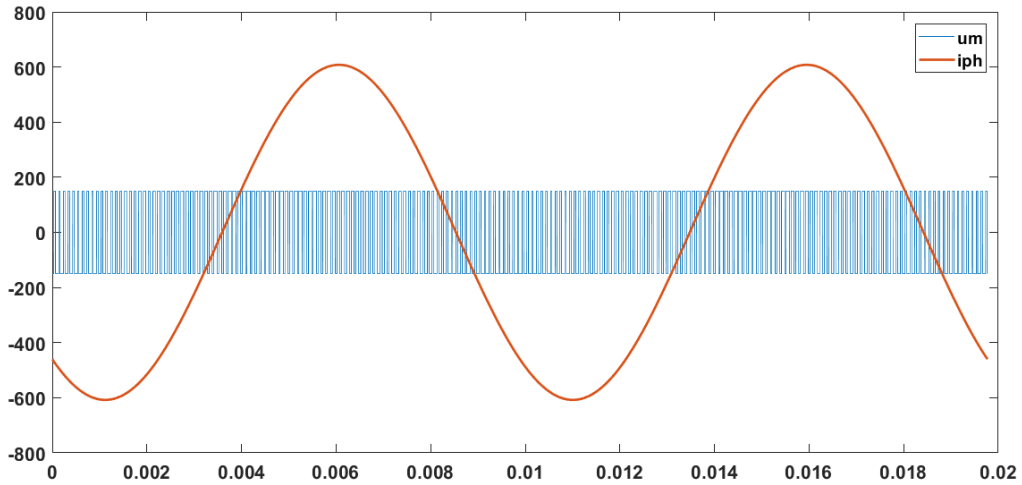

Figure 3.11: Phase to neutral voltage and phase current

It would be enough to explain the operation for one of the phases since the three phases operate with a 120° phase shift to each other. Therefore, one of the phase legs is considered to show the direction of the current flow and the devices that turned on, based on the current and voltage polarities discussed above, as shown in Fig. 3.12.

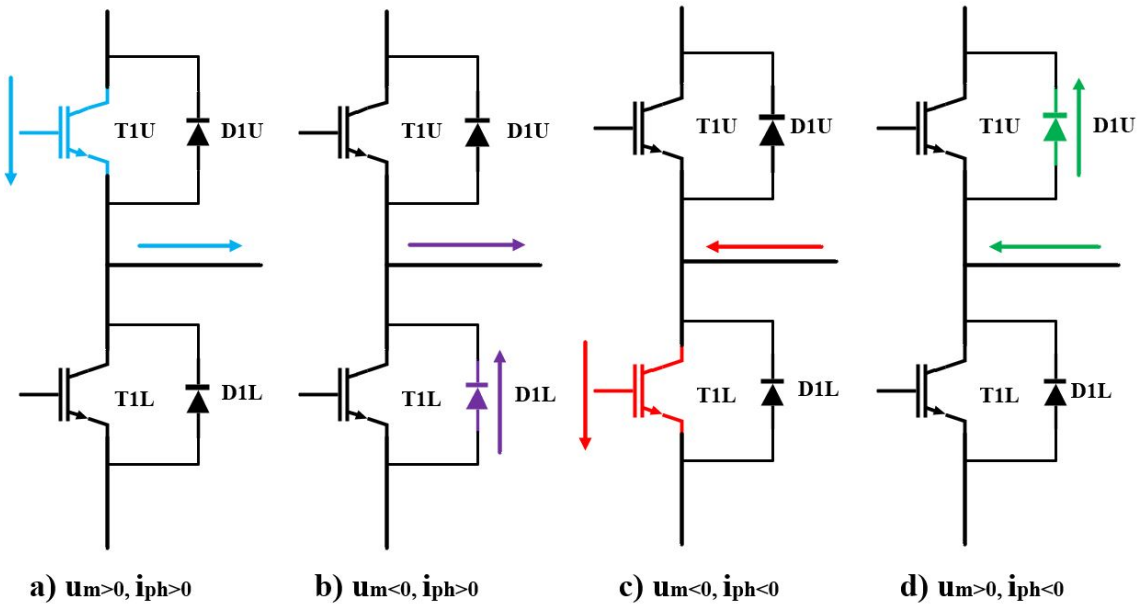

Figure 3.12: Direction of the current and the active switches at different voltage and current conditions

It can be observed from the figure, that during the positive half of the phase current, the upper MOSFET and lower diode conducts. However, during the negative half of the phase current, the lower MOSFET, and upper diode conduct. When voltage and current have the same polarity, only the IGBTs conduct, and if they have different polarities, only diodes conduct.

3.2.2 Three-phase MOSFET inverter with sinusoidal PWM

Without considering the reverse conduction of a MOSFET, the operation principle of the MOSFET inverter is the same as the operation principle of IGBT inverter. Also, the analytical equations for conduction losses are simple to derive.

However, when reverse conduction is considered, in a MOSFET, the operation of the inverter changes. It is known that when the phase to neutral voltage and phase current polarities are opposite, either the upper or lower diode of a phase leg conducts. Yet in MOSFETs, during this condition, both MOSFET and diode conducts only if the product of phase current, i_{ph}, and the on-state resistance, R_{on}, of the MOSFET, is higher than the forward voltage of the diode, V_d. Otherwise only the MOSFET conducts.

To elaborate the above explanation, one of the phase legs of the three-phase inverter is considered and the directions of current flow and switches that are active, based on the polarities of u_m and i_{ph}, are shown in Fig. 3.13

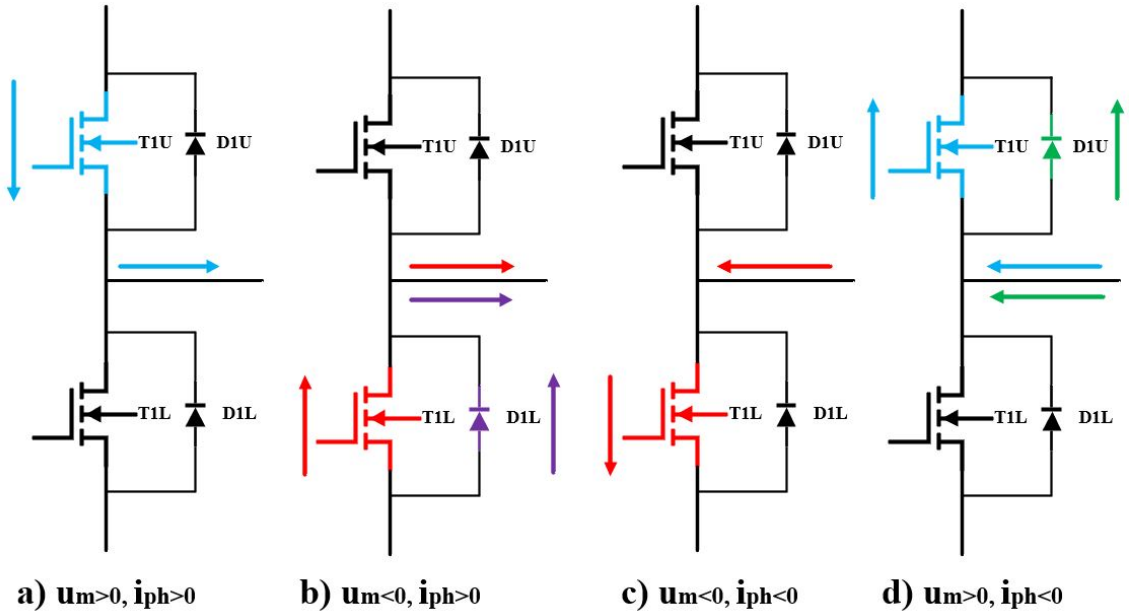

Figure 3.13: Direction of the current and the active switches at different voltage and current conditions

3.3 Analytical Equations for Power Loss Calculation

3.3.1 Analytical equation for calculating conduction losses of IGBT

The conduction losses of an IGBT can be obtained by integrating the product of voltage drop over the device and current flowing through it for half of the fundamental period T_0, because of the symmetry of sinusoidal. Therefore the conduction loss equation is given by

$$P_{cond,IGBT} = \frac{1}{T_0}\int_0^{T_0/2}(V_T + R_f)(Isin(\omega t))^2\tau(t)dt \tag{3.13}$$

where V_T and R_f are the parameters that can be obtained from the output characteristics of the IGBT datasheet. $\tau(t)$ is pulse pattern function which gives duty cycle variation and is given by

$$\tau(t) = \frac{1}{2}(1 + msin(\omega t + \phi)) \tag{3.14}$$

By substituting (3.14) in (3.13) the equation for conduction losses can be rewritten as

$$P_{cond,IGBT} = \frac{1}{2}(V_T.\frac{\hat{I}}{\pi} + R_f.\frac{\hat{I}^2}{4}) + m.cos\phi(V_T.\frac{\hat{I}}{8} + \frac{1}{3\pi}.R_f.\hat{I}^2) \tag{3.15}$$

where m is modulation index, $\hat{I}$ is the peak value of current, ϕ is the phase between voltage and current.

3.3.2 Analytical equation for calculating conduction losses of MOSFET without considering reverse conduction

A MOSFET can be simply modeled as a resistance whereas IGBT is modeled as a voltage source in series with a resistance. Because of the absence of this voltage source in the MOSFET model, when reverse conduction is not considered, the conduction loss can be written as

$$P_{cond,MOSFET} = \frac{1}{T_0}\int_0^{T_0/2} R_{on}(Isin(\omega t))^2\tau(t)dt \tag{3.16}$$

where R_{on} is drain to source on-state resistance.

After substituting pulse pattern function, that is (3.14) in (3.16), the conduction loss in MOSFET can be written as

$$P_{cond,MOSFET} = R_{on}.\hat{I}^2(\frac{\hat{I}}{8} + \frac{m.cos\phi}{3\pi}) \tag{3.17}$$

3.3.3 Analytical equation for calculating conduction losses of Diode

As mentioned in Section 2.5.1, a diode can also be modelled as a resistor in series with a voltage source. Therefore conduction loss equation of diode would be similar to conduction loss equation of IGBT, and is given by

$$P_{cond,Diode} = \frac{1}{2}(V_d.\frac{\hat{I}}{\pi} + R_d.\frac{\hat{I}^2}{4}) - m.cos\phi(V_d.\frac{\hat{I}}{8} + \frac{1}{3\pi}.R_d.\hat{I}^2) \tag{3.18}$$

where V_d and R_d can be obtained from forward characteristics of diode from its datasheet.

3.3.4 Analytical equation for calculating conduction losses of MOSFET and Diode while considering reverse conduction

As mentioned in Section 3.3.2, the conduction loss equation in integral form can be expressed as

$$P_{cond,SiC} = \frac{1}{2\pi}\int_0^{2\pi} R_{on}I_m^2(\alpha)\tau(\alpha)d\alpha \tag{3.19}$$

where α=2π/T and I_m is MOSFET current. $\tau(\alpha)$ is duty cycle or pulse pattern function and is given by

$$\tau(\alpha) = \frac{1}{2}(1 + msin\alpha) \tag{3.20}$$

where m is modulation index. This equation is same as (3.16), except that now it is integrated in terms of radians. During reverse conduction, the MOSFET current and the diode current are given by

$$I_m = \frac{I_m.sin(\alpha - \phi) - V_d}{R_d + R_{on}} \tag{3.21}$$

$$I_d = \frac{I_d.sin(\alpha - \phi) + V_d}{R_d + R_{on}} \tag{3.22}$$

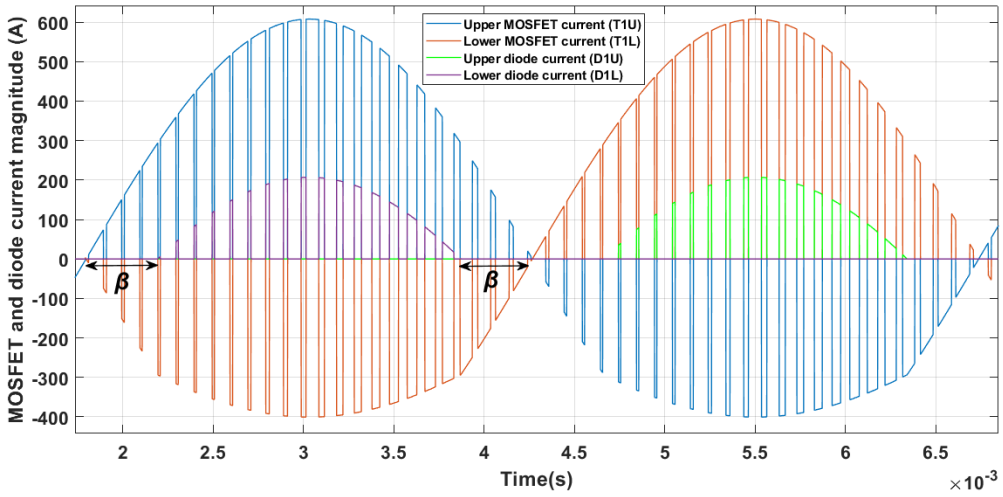

Figure 3.14: Parallel conduction angle during reverse conduction of MOSFET

By replacing ν=$\alpha - \phi$ and substituting (3.20) and (3.21) in (3.19), the MOSFET conduction losses in integral form can be written as [18]

$$P_{cond,MOSFET} = \frac{R_{on}}{4\pi}\left(\int_{-\beta}^{\beta+\pi}(1 + Msin(\nu + \phi))\hat{I}^2 sin^2\nu d\nu + \int_{\beta+\phi}^{-\beta+2\pi}(1 + Msin(\nu + \phi))\left(\frac{R_d\hat{I}sin\nu - V_d}{R_d + R_o n}\right)^2 d\nu\right) \tag{3.23}$$

where β is the parallel conduction angle or the angle from where diode starts to conduct as shown in Fig. 3.14.

$$\beta = sin^{-1}\left(\frac{V_d}{R_{on}\hat{I}}\right) \tag{3.24}$$

Solving the integrals in (3.23) equation for every operating point is a difficult task. Therefore, the solved expression of the above equation can be written as

$$P_{cond,MOSFET} = \frac{R_{on}}{4\pi}\hat{I}^2\left((\pi/2+\beta-\frac{sin2\beta}{2})+2mcos\phi(cos\beta-\frac{cos^3\beta}{3})\right)+$$
$$+\frac{R_{on}}{4\pi(R_{on}+R_d)^2}\left[R_d^2\hat{I}^2\left((\pi/2-\beta+\frac{sin2\beta}{2})-2mcos\phi(cos\beta-\frac{cos^3\beta}{3})\right)+\right.$$
$$\left.+V_d^2\left(\pi-2\beta-2mcos\phi\cos\beta\right)+2R_d\hat{I}V_d\left(2cos\beta-mcos\phi(\pi/2-\beta+\frac{sin2\beta}{2})\right)\right] \tag{3.25}$$

Since MOSFET conducts in parallel with the diode when $\hat{I}$ times R_{on} is greater than V_d, the conduction loss equation of diode also changes. Similar to (3.19) the conduction loss of diode in integral form, can be expressed as

$$P_{cond,diode} = \frac{1}{2\pi}\int_0^{2\pi}(R_dI_d^2(\alpha)+V_dI_d(\alpha))d\alpha \tag{3.26}$$

By substituting (3.20) and (3.22) in (3.26), the diode conduction loss equation can be written as

$$P_{cond,diode} = \frac{R_d}{4\pi}\int_{\beta+\pi}^{-\beta+\pi}(1+msin(\nu+\phi))\left[\left(\frac{R_{on}\hat{I}sin\nu+V_d}{R_d+R_{on}}\right)-V_d\left(\frac{R_{on}\hat{I}sin\nu+V_d}{R_d+R_{on}}\right)^2\right]d\nu \tag{3.27}$$

solving the above equation gives

$$P_{cond,diode} = \frac{R_{on}}{4\pi(R_{on}+R_d)^2}\left[\hat{I}^2R_{on}^2\left(\pi/2-\beta+\frac{sin\beta}{2}-2mcos\phi(cos\beta-\frac{cos^3\beta}{3})\right)\right.$$
$$\left.+V_d^2(\pi-2\beta-2mcos\phi cos\beta)-2\hat{I}R_{on}V_d\left(2cos\beta-mcos\phi(\pi/2-\beta+\frac{sin\beta}{2})\right)\right]$$
$$-\frac{V_d}{4\pi(R_{on}+R_d)}\left[m\hat{I}R_{on}cos\phi(\pi/2-\beta+\frac{sin\beta}{2})+2R_{on}\hat{I}cos\beta-V_d(\pi-2\beta)+2V_dmcos\phi cos\beta\right] \tag{3.28}$$

3.3.5 Switching Losses

Switching losses occur during every turn on and turn off instants of both the switch and its anti-parallel diode. The switching loss is dependent on the switching energy of the device. The switching energies of the Si IGBTs and diodes are relatively higher when compared to SiC devices. Therefore determining switching losses is, of course, essential for determining the total losses of the switches.

The analytical equation to calculate the switching loss is given by

$$P_{sw,IGBT,diode,MOSFET} = f_{sw}.E_{sw}\left[\frac{1}{\pi}.\frac{\hat{i}}{I_{nom}}\right]^{K_i}\left[\frac{V_{dc}}{V_{nom}}\right]^{K_v} \tag{3.29}$$

where E_{sw} is switching energy loss, f_{sw} is switching frequency , V_{nom} ,I_{nom} are nominal voltage and current, K_v and K_i are voltage and current exponents respectively. The above equation to calculate switching loss remains the same for IGBT, diode, and MOSFET. The reverse conduction in MOSFET increases the switching losses, in theory; however, they are negligible[18].

3.4 Thermal Design for IGBT and MOSFET Inverter Modules

In power electronic devices, the junction temperature of the device affects its parameters like on-state resistance $R_T\&R_D$, forward voltage drop $V_T\&V_D$, switching and reverse recovery energies $E_{on}, E_{off}\&E_{rec}$. Therefore it is essential to consider this junction temperature of the device while calculating the power losses associated with the device.

The power losses are calculated for every operating point obtained by following the procedure in Section 3.1.2. Each operating point thus derived has its own current magnitude, modulation index, phase angle, torque, and speed. The operating points at lower torque values have lower current magnitudes, due to which the device's junction temperature would not be much higher than the fluid temperature in the case of automotive applications. However, operating points at higher torque values have higher current magnitudes, which makes the device's junction temperature go high than the fluid temperature. As mentioned before, that this high junction temperature changes the device parameters.

Therefore the junction temperature of the device has to be considered for the accurate calculation of power losses. The junction temperature calculation procedures of IGBT and MOSFET are shown in Figs. 3.15 & 3.16

For automotive application IGBT modules, the junction to fluid thermal resistance is directly provided in the datasheet. However, for IGBT and MOSFET modules used for the motor drive and other applications, usually the junction to case and case to sink thermal resistances are provided in the datasheet. In this thesis work, an attempt is made to observe how the power losses would be if these non-automotive IGBT/MOSFET modules are used in the automotive application. Therefore a water-cooled heat sink is used instead of a natural air-cooled heat sink. In Fig. 3.16 case

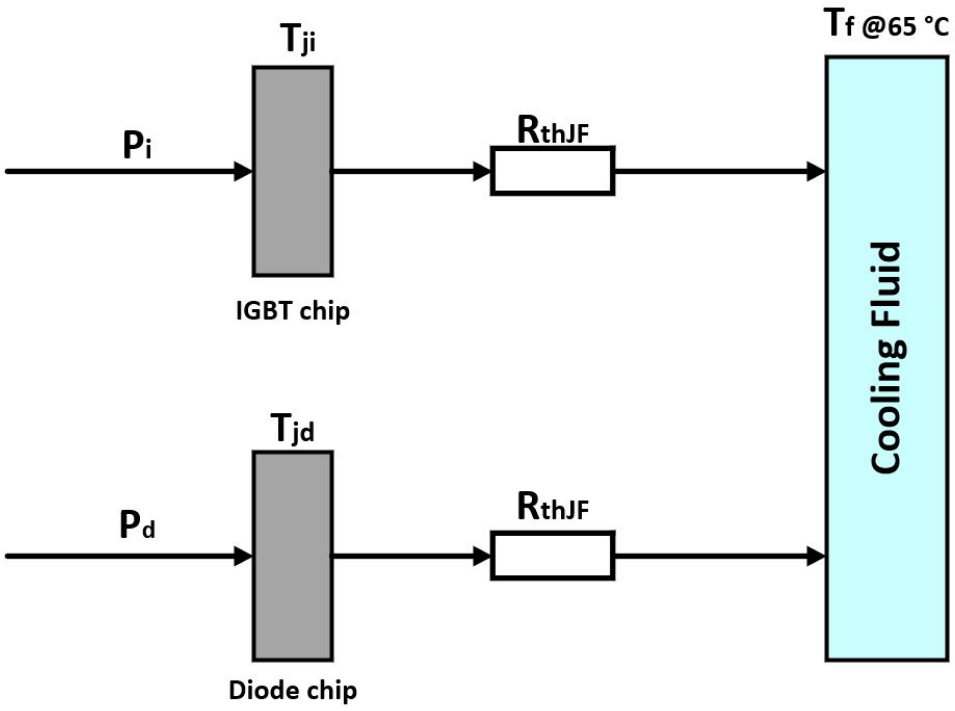

Figure 3.15: Junction temperature calculation of automotive IGBT modules

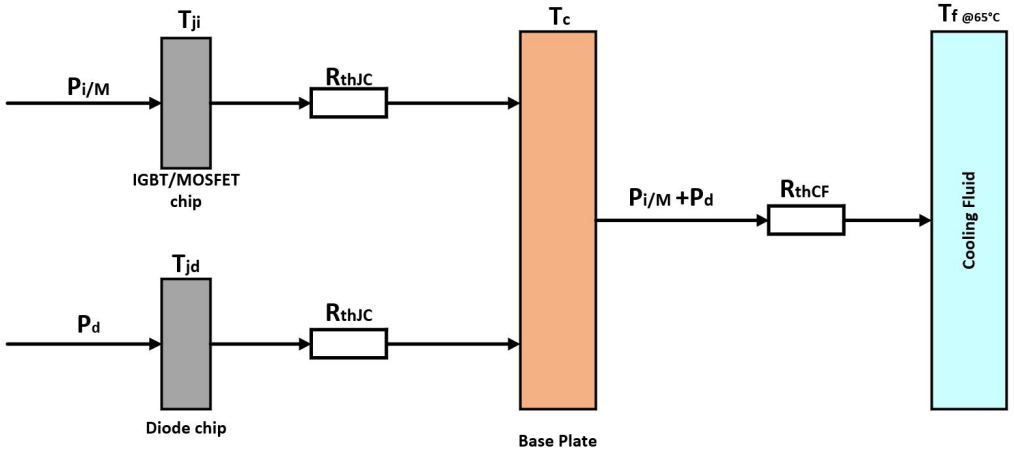

Figure 3.16: Junction temperature calculation of motor drive and other application IGBT/MOSFET modules [19]

to fluid thermal resistance is the sum of the case to sink and sink to fluid thermal resistance, but due to lack of availability of case to sink thermal resistance value, it is neglected.

The inclusion of junction temperature effect in device parameter calculation is explained as follows. At first, the device parameters are taken at 65°C, which is

the same as the fluid temperature. These parameters are used in the analytical power loss equations mentioned in Section 3.3. Thus the obtained power losses are multiplied with the junction to fluid thermal resistance, in the case of automotive IGBT modules, to obtain the temperature flowing from junction to fluid. For non-automotive IGBT modules, this temperature is obtained, as shown in Fig. 3.16. If the fluid temperature is added to this temperature, then it becomes the actual device's junction temperature, which will be higher than the junction temperature assumed before.

Using this newly obtained junction temperature, the device parameters and the power losses can be recalculated. If this process is repeated for a few times, as shown in the Fig. 3.17, the convergence of power loss can be observed as shown in Fig. 4.12

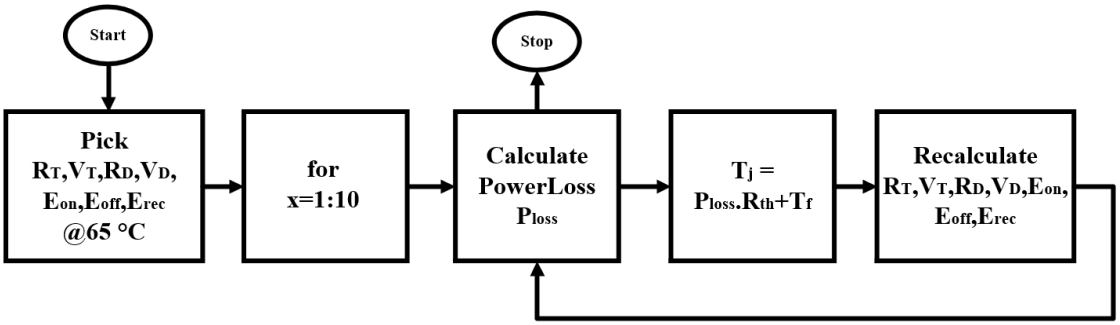

Figure 3.17: Thermal design flowchart to find the the power loss at a steady-state

3.5 Reference Voltages Using THIPWM

In this section, the method of the third harmonic injection into the reference voltage is described. The third harmonic injection signal increases the available maximum output voltage of an inverter by 15.5 percent, as given by

$$V_{max} = \frac{V_{dc}}{\sqrt{3}} \tag{3.30}$$

$$V_{3rd} = \frac{V_{max} + V_{min}}{2} \tag{3.31}$$

where in (3.31), V_{max} and V_{min} are the maximum and minimum values of the three-phase sinusoidal reference voltage. Thus, after the injection of third harmonic voltage, the resultant three-phase reference voltages can be written as

$$u_{aref} = \hat{U} \sin wt - V_{3rd} \tag{3.32}$$

$$u_{bref} = \hat{U} \sin wt - 120° - V_{3rd} \tag{3.33}$$

$$u_{cref} = \hat{U} \sin wt - 240° - V_{3rd} \tag{3.34}$$

3.6 Life-Cycle Cost Analysis Model

An LCCA model with a reasonable approximation of the costs involved over the lifetime of the inverters is derived. Operating costs which include labor and running costs, as well as maintenance costs, are not included in this LCCA model. Therefore, further discussion only deals with purchase cost and Net Present Value (NPV) of the energy losses in the power converter over its lifetime. Also, the cost of the cooling system needed to dissipate the heat generated in the inverters is included.

A comparative LCCA model for CAS300M12BM2 SiC MOSFET inverter and FZ600-R12KE3 Si IGBT inverter is developed to asses their performance. The LCCA model includes the cost of the power inverters and cooling system as well as the cost of the total energy losses in the power converters over a defined lifetime, as shown in Fig. 3.18.

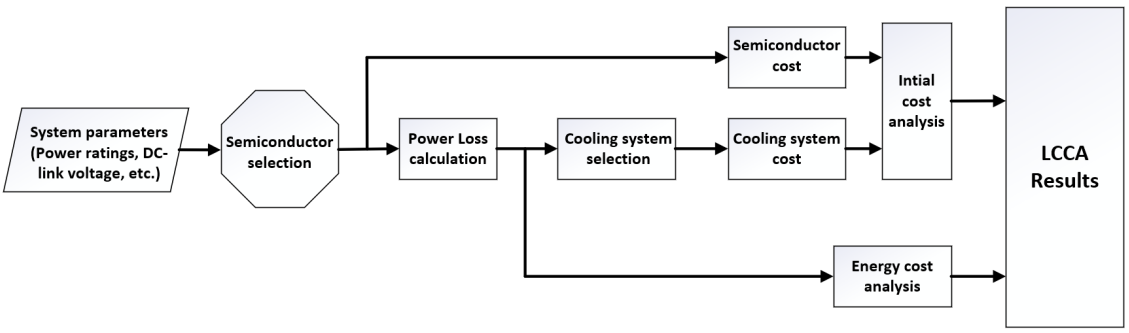

Figure 3.18: The procedure for developing the LCCA model for the power inverter in the PMSM drive system[16]

At present, the cost of the SiC MOSFET inverter is higher than the FZ600R12KE3 Si IGBT inverter cost, so two different kinds of price dependent analyses are presented in this thesis for showing the effect of varying purchase prices over a period of time. The LCCA model, based on the present price of the SiC MOSFET inverter is considered as the high-cost scenario model, whereas the one which is based on the anticipated future price, which is lesser than the present price, is considered as the low-cost scenario model.

There are some limitations in finding the exact price of the entire life of an asset due to the varying degree of uncertainty in prices associated with economic or other factors such as

- The usage pattern of the asset over time
- The way course of operating costs change

- The necessity and cost of maintenance
- The influence of inflation and interest rate, where the inflation rate is a sustained change in the prices of the goods over a period of time
- The estimation of the asset's useful life

3.6.1 Driving cycle

The energy losses of the inverters are calculated by assuming that a car, with specifications mentioned in Table 3.2, is driven on the City Manual (ECE) part of the New European driving cycle (NEDC) profile throughout its entire lifetime. The lifetime of the inverters is assumed 20 years, and it is further assumed that the power inverters are used for half of the total lifetime.

Quasi Static Simulation (QSS) is a toolbox that makes the designing of a powertrain system simple. The ECE driving cycle profile is generated by using the QSS toolbox, as shown in Fig. 3.19.

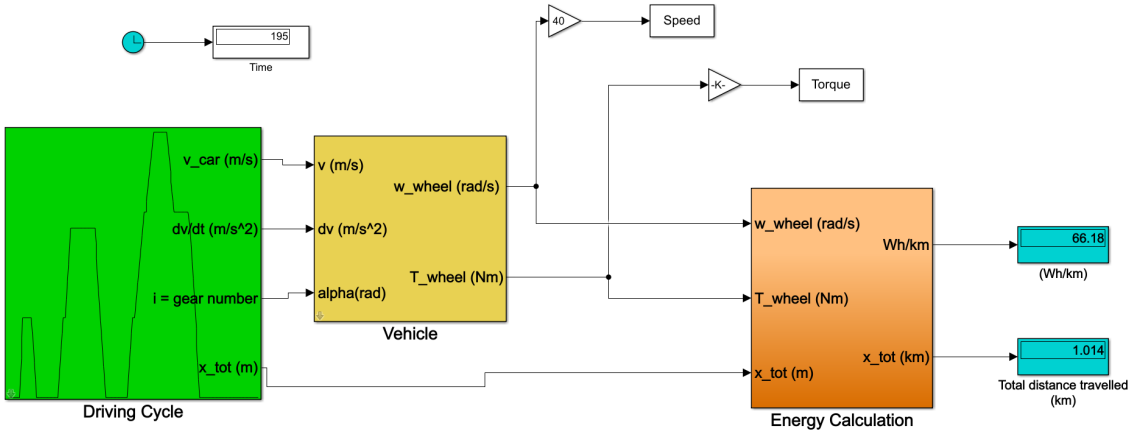

Figure 3.19: Simulation model for generating the driving cycle in the QSS toolbox

Table 3.2 presents the parameters of the selected car, which are used in the above shown QSS model to obtain the torque values corresponding to the speeds in the driving cycle.

Table 3.2: Car parameters to generate a driving cycle profile in QSS toolbox

Name	**Unit**	**Value**
Total mass of car	m	1700 kg
Aerodynamic drag coefficient	C_d	0.7
Vehicle cross section area	A	2 m^2
Rolling friction coefficient	C_r	0.007
Wheel radius	r	0.3 m
Gear ratio	i	1:10

The ECE driving cycle is shown in Fig. 3.20 and torque corresponding to the speed of this driving cycle is shown in Fig. 3.21. The values of i_{sd}, i_{sq}, ψ_{sd} and ψ_{sq} corresponding to the driving cycle's speed and torque are calculated by using interpolation function in MATLAB.

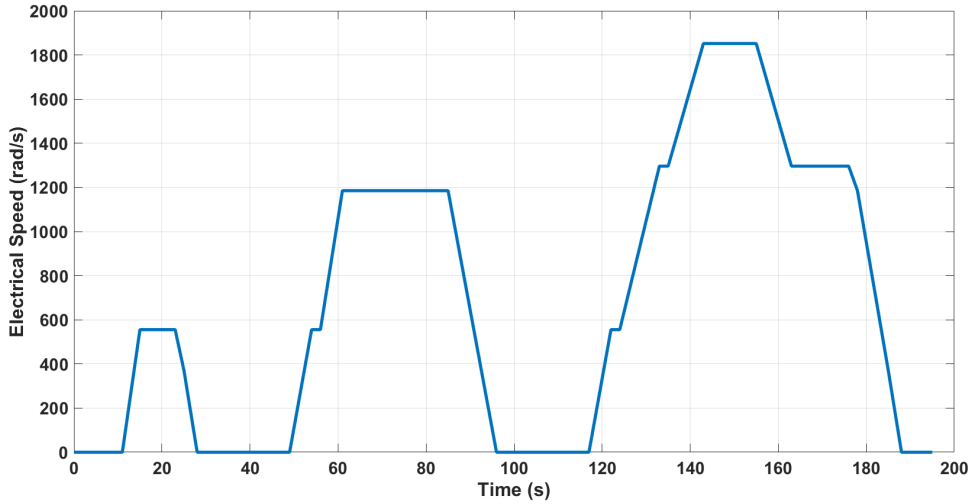

Figure 3.20: Europe city manual (ECE) driving cycle

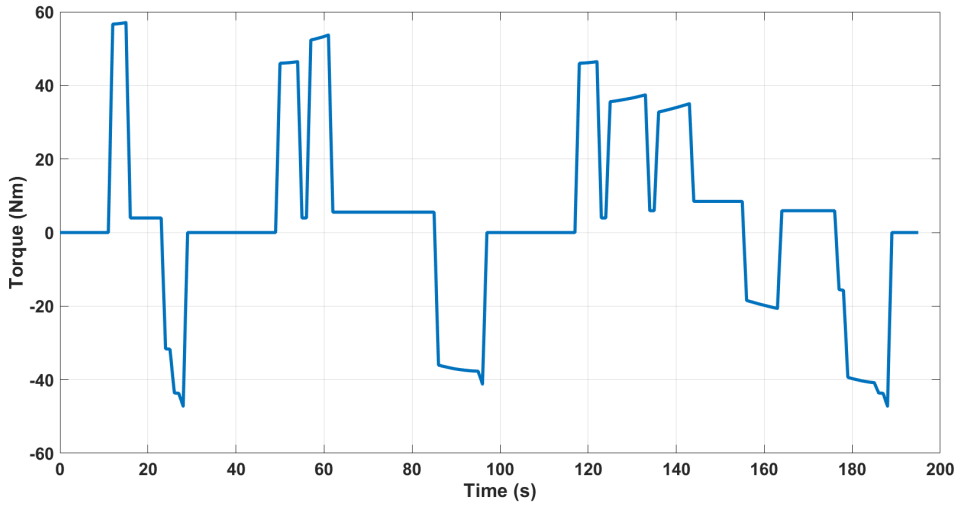

Figure 3.21: Torque corresponding to ECE driving cycle

3.6.2 Net Present Value (NPV)

The power losses of the SiC MOSFET inverter and Si IGBT inverter corresponding to the driving cycle, mentioned in the previous section, are calculated by using the equations presented in Section 3.3 and the energy cost is calculated based on the electricity price. The discount rate, which comprises of inflation and interest rate, of 2.5 percent is used to calculate the present value of the future expenditure as given by

$$PV = \frac{FV}{(1+r)^n} \tag{3.35}$$

where PV is the present value, FV is the future value, r is the discount rate, and n is the number of years. The present value of costs associated with the life cycle of the inverters is derived by cumulative summation of the present value of each year individually.

Net Present Value (NPV) is the sum of all the present values of all cash flows associated with a project[20]. The NPV is a valuable tool to analyze an investment decision which gives the company/firm an explicit option to forecast if the investment builds on value to the company. The NPV of the energy losses of the inverters can be calculated as

$$NPV = \sum_{n=1}^{N_{life}} \frac{C_{eng,n} E_{loss,n}}{(1+r)^n} \tag{3.36}$$

where r is the discount rate, and it varies for each company depending on the way of funding and other factors. n is the number of the year, $C_{eng,n}$ is the price of the

energy per unit(kWh) which is 3 kronor, in Swedish currency, N_{life} is the total life time of the converter, $E_{loss,n}$ is the total energy loss over a specified time period.

3.6.3 Initial cost

The initial cost of a power converter includes the purchase cost of the converter and its cooling system components. The cost of the power converters can be calculated from the vendor websites like digikey.se. The initial cost of the CAS300M12BM2 SiC MOSFET half-bridge module and FZ600R12KE3 Si IGBT discrete module are given in Table 3.3. It can be seen that the SiC MOSFET module is more expensive than the Si IGBT module due to its high material cost, high manufacturing cost, high demand, and low availability.

Table 3.3: Purchase cost of the chosen modules

Inverter	**Ratings**	**Manufacturer**	**Price of a module (kr)**	**Price for a 3-phase inverter (Kr)**
CAS300M12BM2 SiC MOSFET	1200 V 600 A	CREE	5,441	16,323
FZ600R12KE3 Si IGBT	1200 V 600 A	Infineon	1,290	7,740

4

Results & Discussion

This following section will present the simulation results of the drive system model which was developed in previous chapter.

4.1 Simulation Model for Control of Non-linear PMSM and Analysis

By following the procedure mentioned in Section 3.1, a drive system model is built using MATLAB/Simulink. The speed controller is not included in this drive system since the main interest is to check the working/performance of the torque controller. The Simulink model of the total drive system is as shown in Fig. 4.1

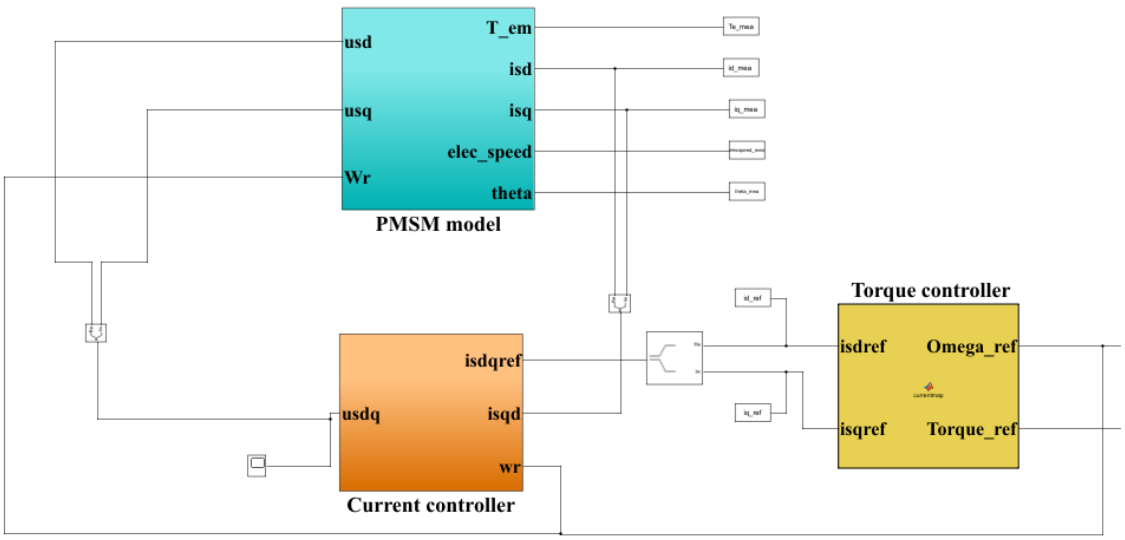

Figure 4.1: PMSM drive system

To evaluate the working of the drive system, the torque reference is given as shown in Fig. 4.2, Where the measured torque following the reference can also be seen, and the speed input is given as in Fig. 4.3. The torque reference and speed input are given in a way that with an increase in speed the torque reduces or vice versa. The speed input is given as a ramp signal with a certain slope such that the signal

reaches around 4800 RPM in one minute. As there is no speed controller, the speed can only be given as input, but can't be controlled.

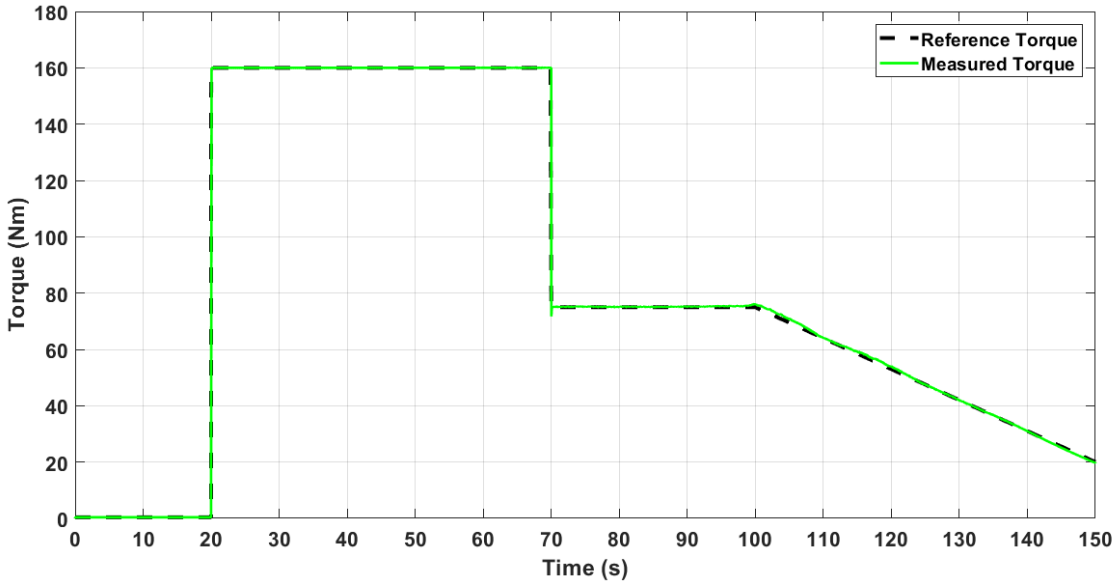

Figure 4.2: Reference torque (Black-Dashed) Vs Measured Torque (Green)

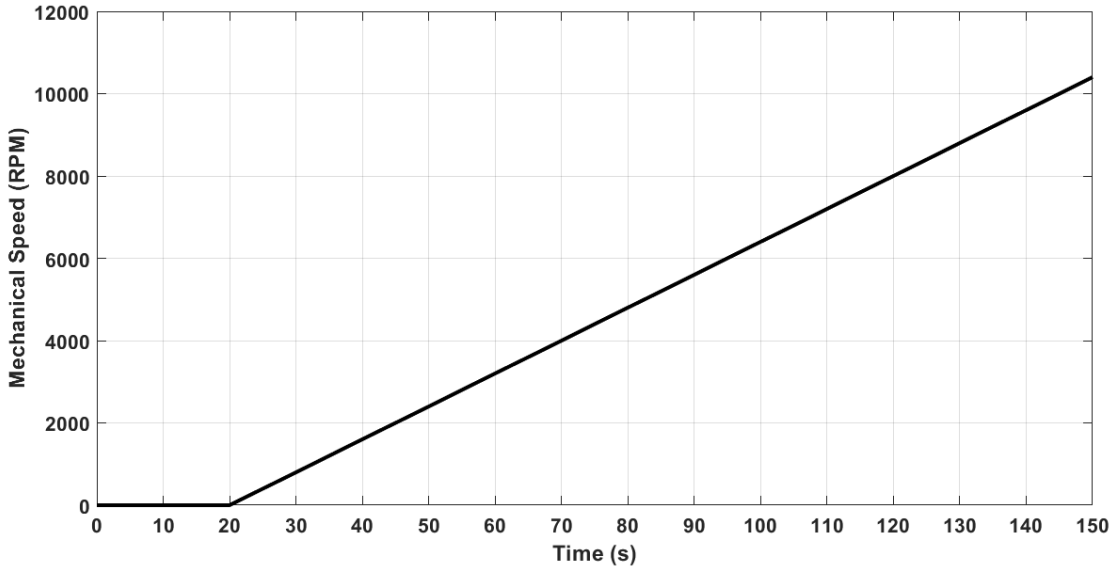

Figure 4.3: Mechanical Speed Input

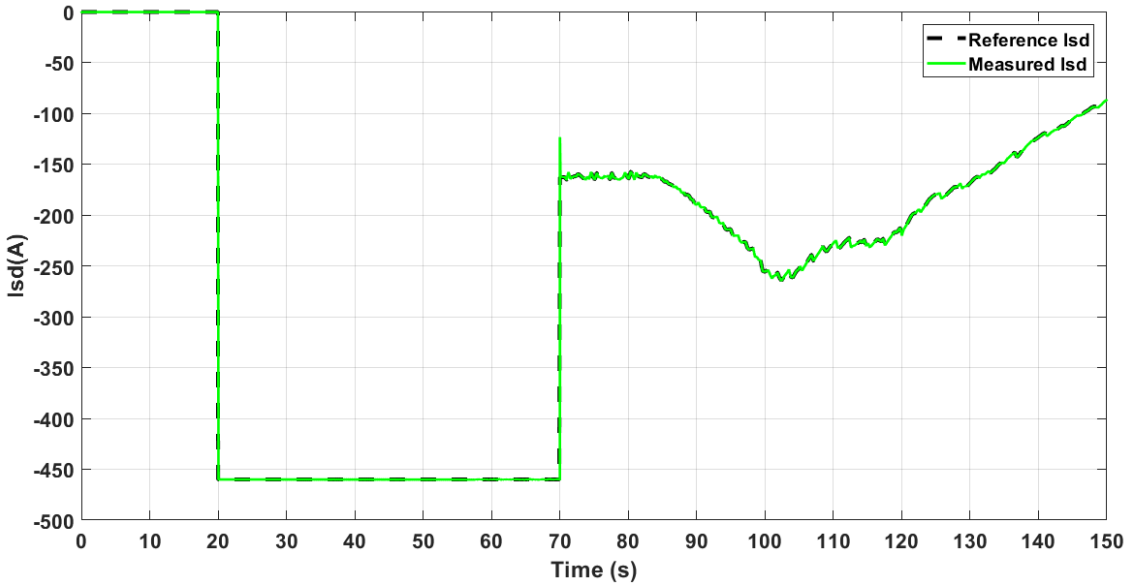

Figure 4.4: Reference i_{sd} Vs Measured i_{sd}

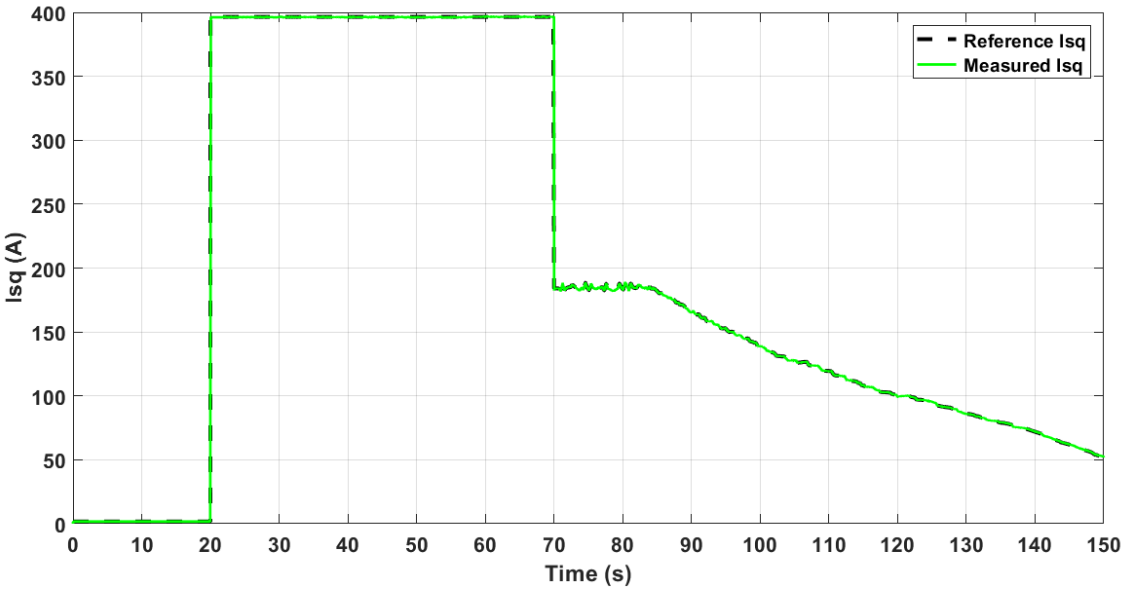

Figure 4.5: Reference i_{sq} Vs Measured i_{sq}

Fig. 4.2 shows that reference torque or the measured torque is 160Nm from 20 to 70 seconds, during this time the machine speed reached to 4000 RPM. Between this time, it can be observed that i_{sd} and i_{sq} values are staying almost constant; this means that the PMSM can deliver this torque even though the speed is increasing. Because, during this time, speed is not a limitation for PMSM to deliver the

demanded torque, since the back-emf induced by the rotor is less than the voltage limit. Therefore, the machine is operating in the MTPA region during this period.

The zoomed-in picture at 70 to 100 seconds of measured i_{sd} and measured i_{sq} is shown in Fig. 4.6. The torque demand during this time is 75 Nm, and the speed is changing from 4000 to 6400 RPM. It can be observed in this figure that i_{sd} & i_{sq} stayed constant until around 85 seconds, where the speed is around 5200 RPM, which means that the motor is still operating in MTPA region, due to reduced torque demand. From then i_{sd} starts to increase, and i_{sq} starts to decrease in magnitude.

Producing 75 Nm of torque at speed ranging from 5200 to 6400 RPM is not possible without increasing i_{sd} and reducing i_{sq} magnitudes. Therefore, now the operating point is in constant power region, also it can be observed that the rate of increase of i_{sd} in more than the rate of decrease of i_{sq}.

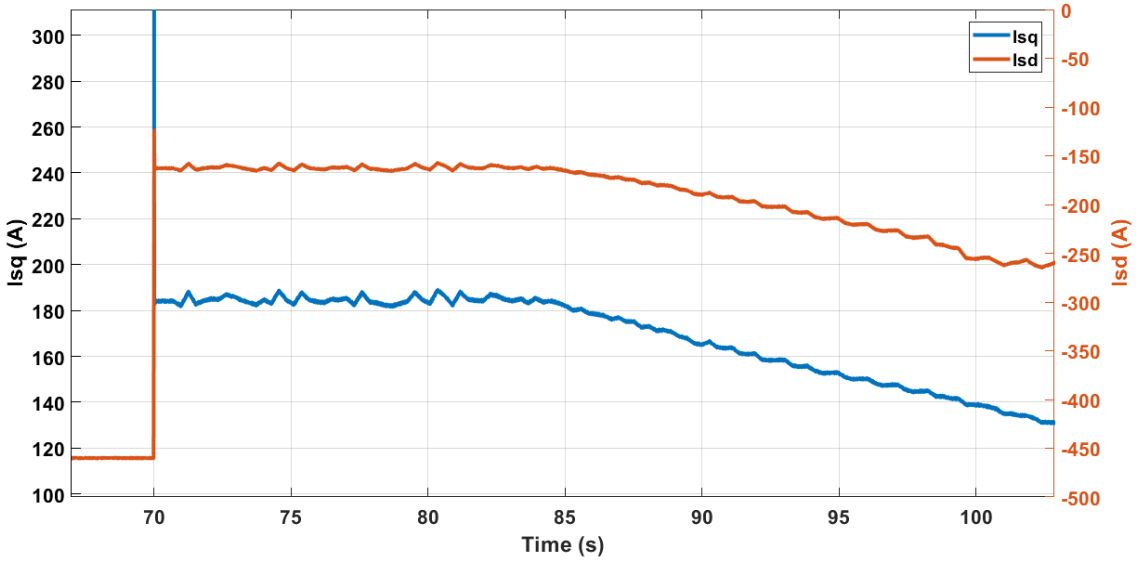

Figure 4.6: Measured i_{sd} and i_{sd} zoomed at 70 to 100 seconds

Fig. 4.7 shows the zoomed-in picture of measured i_{sd} & i_{sq} from 100 to 150 sec, during this speed the speed is increasing from 6400 RPM to 10400 RPM. To explain the concept of MTPV, the torque demand is reduced with a negative slope, which can be seen in Fig. 4.2, since delivering a constant torque demand is not possible at this speed. Unlike previous cases here both i_{sd} & i_{sq} are decreasing in magnitude. From this observation, this machine can be considered theoretically as an infinite speed drive, which means the maximum current of this PMSM is less than its short circuit current, which can be observed in Fig. 3.8. By reducing the magnitudes of i_{sd} & i_{sq}, the machine speed can be increased to higher values. However, the torque demand has to be reduced.

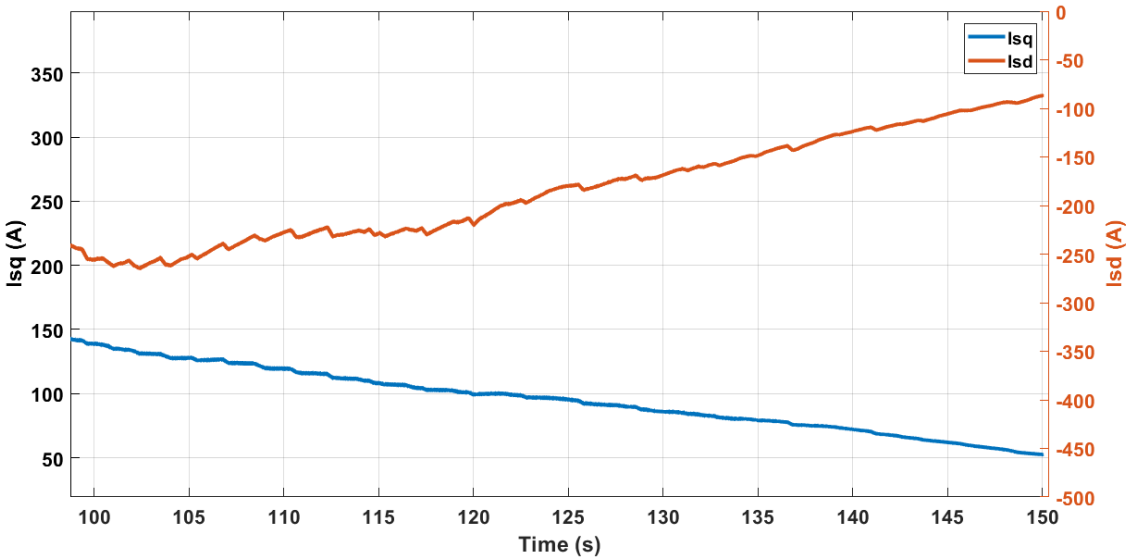

Figure 4.7: Measured i_{sd} and i_{sd} zoomed at 100 to 150 seconds

i_{sd}, i_{sq} contours on speed-torque map are shown in Figs. 4.8 & 4.9. By projecting Fig. 4.2 on these figures, the behaviour of i_{sd} and i_{sq} in MTPA, constant power and MTPV regions can be understood.

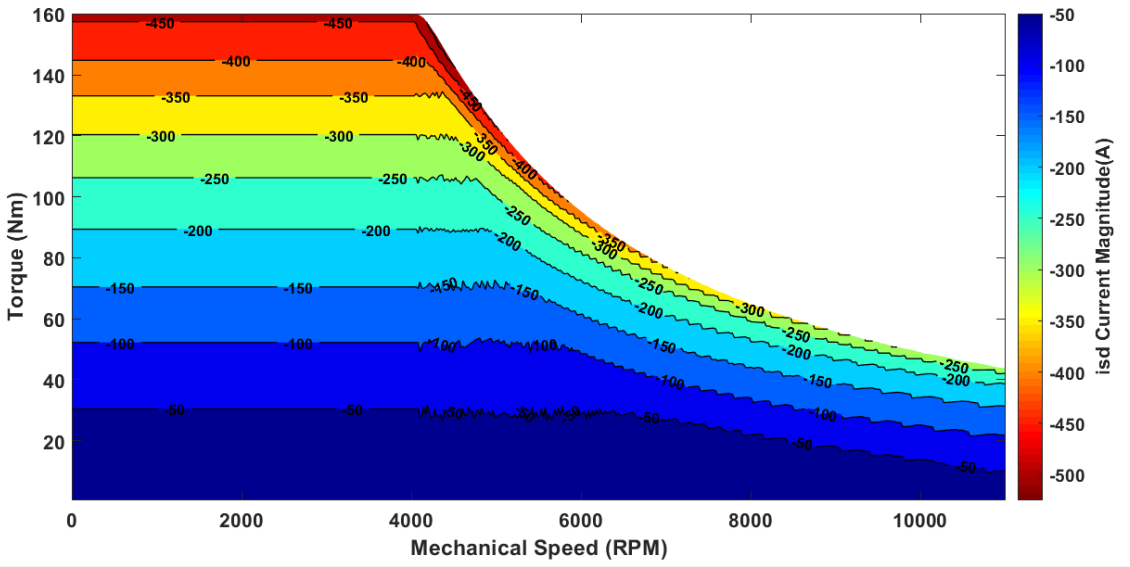

Figure 4.8: i_{sd} contours on speed-torque map

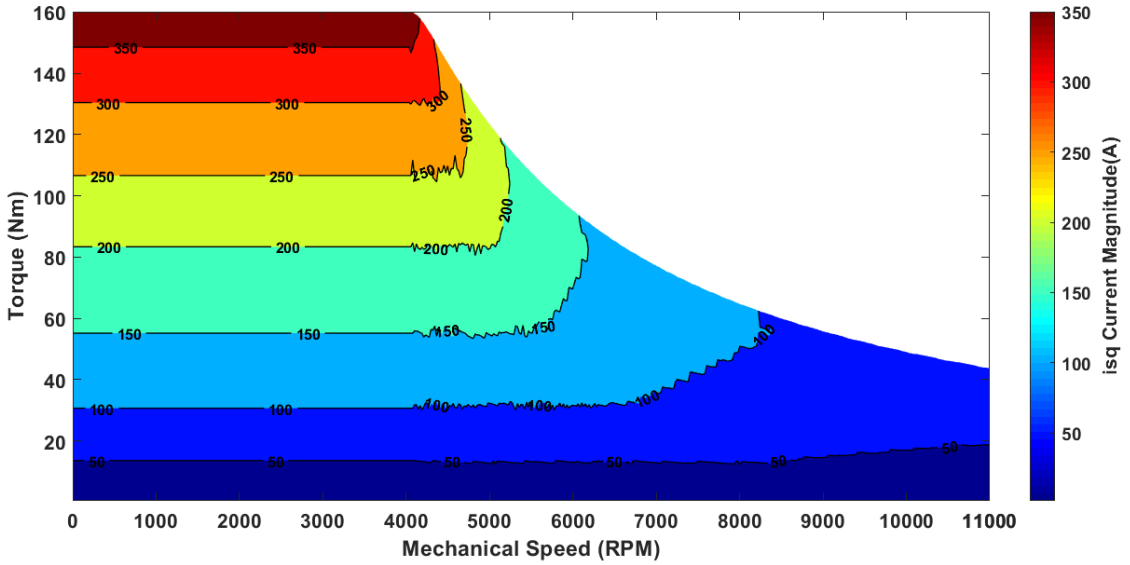

Figure 4.9: i_{sq} contours on speed-torque map

Instead of giving torque input in the form of steps and slope, now the torque input is given as 40Nm constant value. The variation in i_{sd} and i_{sq} with respect to speed at this torque input is shown in Fig. 4.10

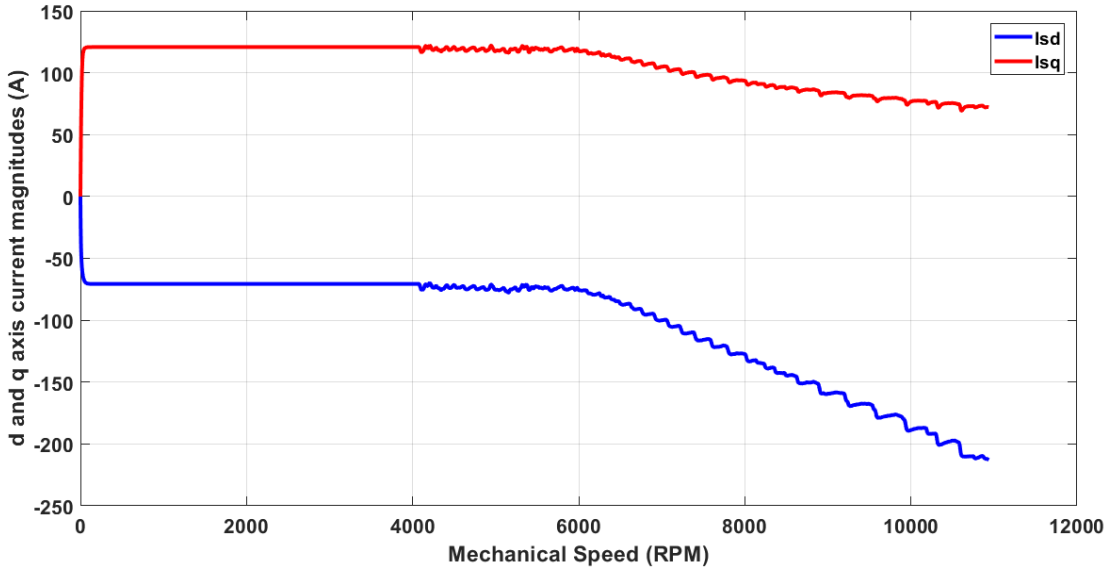

Figure 4.10: i_{sd} and i_{sq} at 40Nm torque input

i_{sd} and i_{sq} are almost staying constant until around 6000RPM; this means that until 6000RPM the flux ellipse is large enough, and more negative d-axis current need not to be provided to produce this torque. Whereas when the speed crosses 6000RPM,

more negative d-axis current, than required, needs to be provided to generate a 40Nm torque without crossing the voltage limit. Here the torque demand is low enough that it need not be reduced to operate the machine in high-speed operation region.

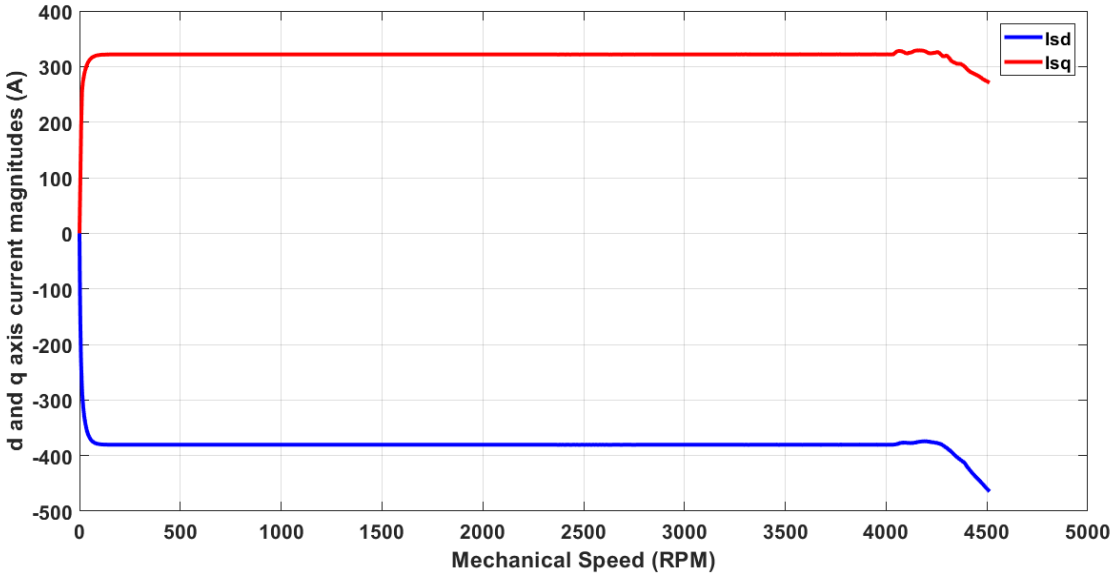

Figure 4.11: i_{sd} and i_{sq} at 140Nm torque input

i_{sd} and i_{sq} magnitudes at 140Nm constant torque input are shown in Fig. 4.11. Here i_{sd} and i_{sq} are constant only until around 4250RPM, the flux ellipse constraint comes into the picture quicker than before, since the torque demand is high. Until 4250RPM the motor was operating in the MTPA region, however after this speed i_{sd} starts to increase and i_{sq} starts to decrease to operate the motor without crossing the voltage limit. After, 4500RPM the simulation stops, since torque demand has to be reduced to operate the motor beyond 4500RPM. If the torque demand is reduced after at 4500RPM, the behavior of i_{sd} and i_{sq} would be as shown in Fig. 4.7.

4.2 Power Losses of Three-Phase IGBT and MOSFET Inverters with and without Thermal Design

For comparing the power losses, the IGBTs chosen are FS600R07A2E3 & FZ600R12KE3 manufactured by Infineon technologies and the SiC MOSFET chosen is CAS300M12BM2 manufactured by Wolfspeed (Formerly CREE). FS600R07A2E3 is an IGBT module which is mainly used in automotive & HEV applications, it has a blocking voltage of 650V and is suitable for the DC link voltage level considered in this work, but SiC MOSFETs are generally designed to block higher voltage levels. So to have a fair comparison, the FZ600R12KE3 IGBT module is chosen, which has a blocking voltage of 1.2KV, which is equal to CAS300M12BM2 MOSFET's blocking voltage, both these devices are used for non-automotive applications. So, in this thesis work an attempt is made to check how the losses would be when FZ600R12KE3 IGBT and CAS300M12BM2 MOSFET modules are used for automotive applications.

The purpose of this section is also to show how the device's junction temperature affects the power losses associated with it. Therefore for comparing power losses, an operating point is chosen where the current magnitude is high. The details of the operating point are provided in Table 4.1

Table 4.1: Details of the chosen operating point for power loss comparison

Name	Value
Torque	160.09 Nm
Electrical Speed	1517 RPM
i_{sd}	-460.42 A
i_{sq}	397 A
Current Magnitude	608 A
ψ_{sd}	-26.9mWb
ψ_{sq}	81.1mWb
Modulation Index	0.1358
f_{sw}	10KHz

4.2.1 Power loss calculation and analysis of FS600R07A2E3 IGBT Inverter

This IGBT module has a blocking voltage of 650V, and the nominal current rating is 400A. The total losses in this inverter comprise the conduction and switching losses of 6 IGBTs and 6 diodes. By using the analytical equations mentioned in Section 3.3, the switching and conduction losses of both IGBT and diode can be derived. The results of device parameters and power loss values are shown in Tables. 4.2 and 4.3 respectively. T_j assumed column consists of the device parameter and power loss values when the junction temperature of both IGBT and diode is assumed as 65°C, which is equal to cooling fluid temperature. Whereas, T_j actual column consisted of device parameter and power loss values when junction temperatures of both IGBT and diode reached steady state. After implementing the thermal design, the steady-state junction temperatures of IGBT and diode are 108.4°C and 91.72°C respectively

Table 4.2: Device parameters at assumed and actual device junction temperatures, R_f = On-state resistance of IGBT, V_T= On-state voltage drop of IGBT, R_d= Forward resistance of diode, V_d= Forward voltage drop of diode, E_{on}= Switch on energy loss of IGBT, E_{off}= Switch off energy loss of IGBT, E_{rec} = Reverse recovery energy of diode

Name	**At assumed T_j**	**At actual T_j**	**Diff.**	**Diff.(%)**
R_f	1.5mΩ	1.7mΩ	0.2mΩ	13.33
V_T	0.73V	0.66V	-0.07V	-9.58
R_d	1.2mΩ	1.3mΩ	0.1mΩ	8.33
V_d	0.85V	0.8V	-0.05V	-5.88
$E_{on} + E_{off}$	40mJ	42.2mJ	2.2mJ	5.5
E_{rec}	5.1mJ	7mJ	1.9mJ	37.25

Table 4.3: Power Losses of FS600R07A2E3 inverter at assumed and actual junction temperatures temperatures

Name	**At assumed T_j (W)**	**At actual T_j (W)**	**Diff.(W)**	**Diff.(%)**
IGBT cond. loss	906.23	946.65	40.42	4.46
IGBT swit. loss	1160	1223	63	5.43
Diode cond. loss	761.01	740.89	-20	-2.64
Diode swit. loss	147.48	202.39	54.91	37.23
Total loss	2975.5	3113.7	138.2	4.64

These tables show that the device's parameters change with respect to junction temperature, and this parameter variation results in the variation of power losses. It can be observed that the total losses of the module are 2975.5 W at assumed junction temperature, whereas it reached a steady-state value of 3113.7 W after thermal design implementation. There is an increment of 138W power loss.

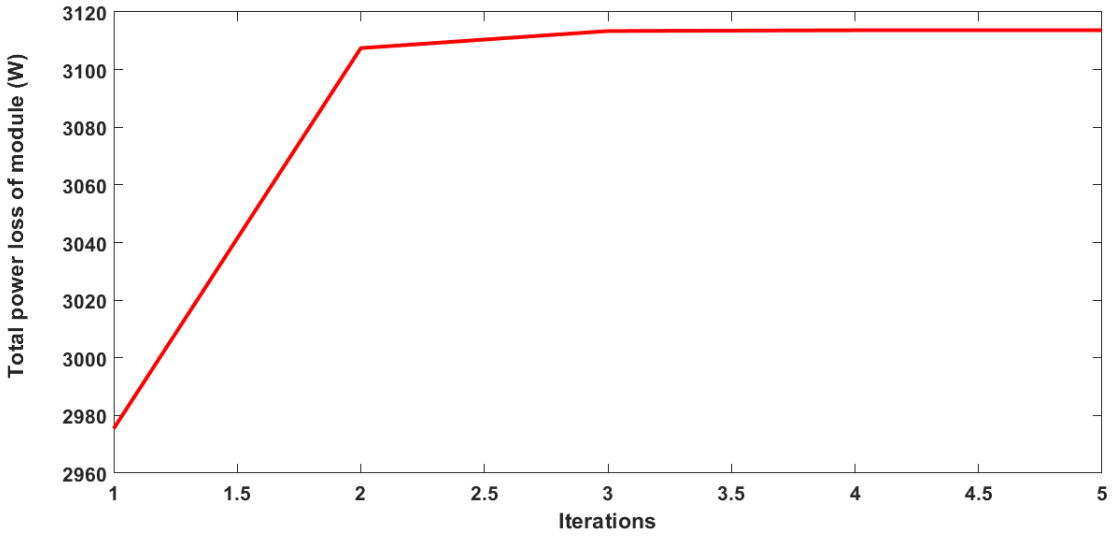

Figure 4.12: Power Loss Convergence in FS600R07A2E3 IGBT inverter

By following the procedure mentioned in Section 3.4, the junction temperature effect is included in power loss calculation, and the power loss convergence is shown in Fig.

4.12. The total losses of the module at every operating point after implementing thermal design is as shown in the Fig. 4.13

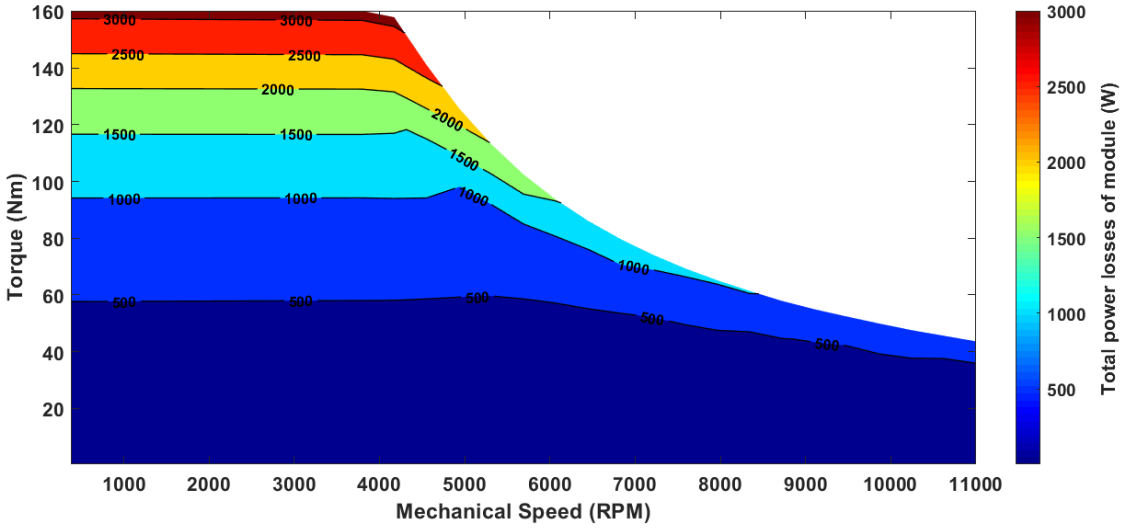

Figure 4.13: Total losses at all the operating points for FS600R07A2E3 IGBT

4.2.2 Power loss calculation and analysis of FZ600R12KE3 IGBT inverter

This IGBT has a blocking voltage level of 1200V, and the nominal current rating is 600A. The same analytical equations mentioned in Section 3.3 are used here to calculate the power losses. The power loss and device parameters before and after reaching steady-state value are shown in Tables. 4.4 and 4.5. The steady-state values of IGBT and diode junction temperatures are 87.79°C and 91.29°C respectively.

Table 4.4: Device parameters at assumed and actual junction temperatures, R_f = On-state resistance of IGBT, V_T= On-state voltage drop of IGBT, R_d= Forward resistance of diode, V_d= Forward voltage drop of diode, E_{on}= Switch on energy loss of IGBT, E_{off}= Switch off energy loss of IGBT, E_{rec} = Reverse recovery energy of diode

Name	**At assumed T_j**	**At actual T_j**	**Diff.**	**Diff.(%)**
R_f	1.5mΩ	1.7mΩ	0.2mΩ	13.33
V_T	0.8V	0.79V	-0.01V	-1.25
R_d	1.3mΩ	1.4mΩ	0.1mΩ	7.69
V_d	0.88V	0.82V	-0.06V	-6.81
$E_{on} + E_{off}$	111.3mJ	122.2mJ	10.9mJ	9.79
E_{rec}	37.8mJ	44.1mJ	6.3mJ	16.66

Table 4.5: Power Losses of FZ600R12KE3 IGBT inverter as assumed and actual junction temperatures

Name	**At assumed T_j (W)**	**At actual T_j (W)**	**Diff. (W)**	**Diff.(%)**
IGBT cond. loss	975.26	1009	24.74	3.45
IGBT swit. loss	844.63	927.06	82.43	9.75
Diode cond. loss	800.04	788.50	-11.54	-1.44
Diode swit. loss	481.99	562.88	80.89	16.78
Total loss	3101.9	3288.0	186.1	5.99

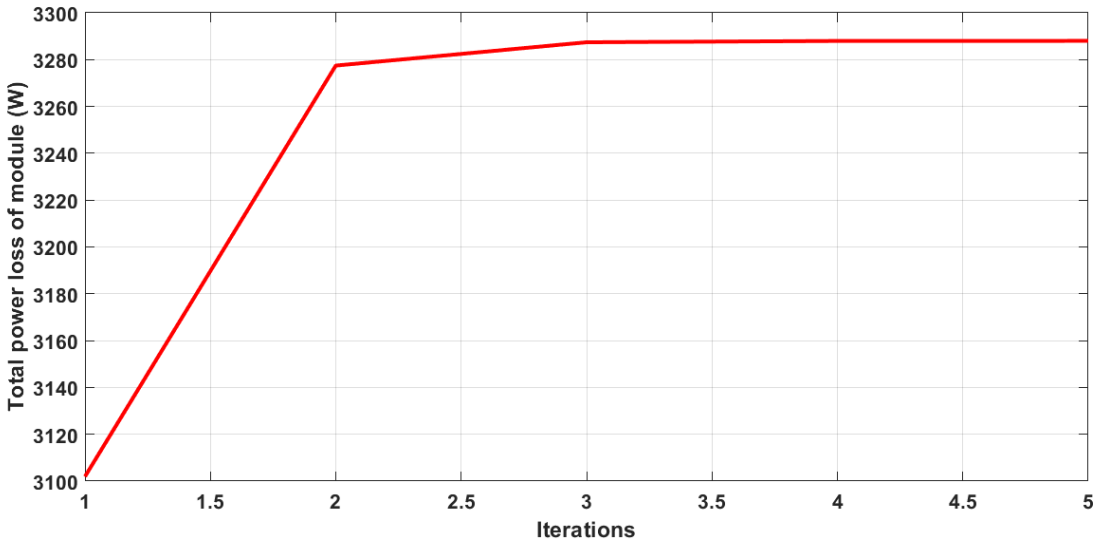

Figure 4.14: Power Loss Convergence in FZ600R12KE3 IGBT inverter

In this IGBT inverter, there is 186.1W of power loss increment at steady state. Which can also be seen in Fig. 4.14. Fig. 4.15 shows the total losses of IGBT inverter at different torque-speed combinations, after implementing the thermal design

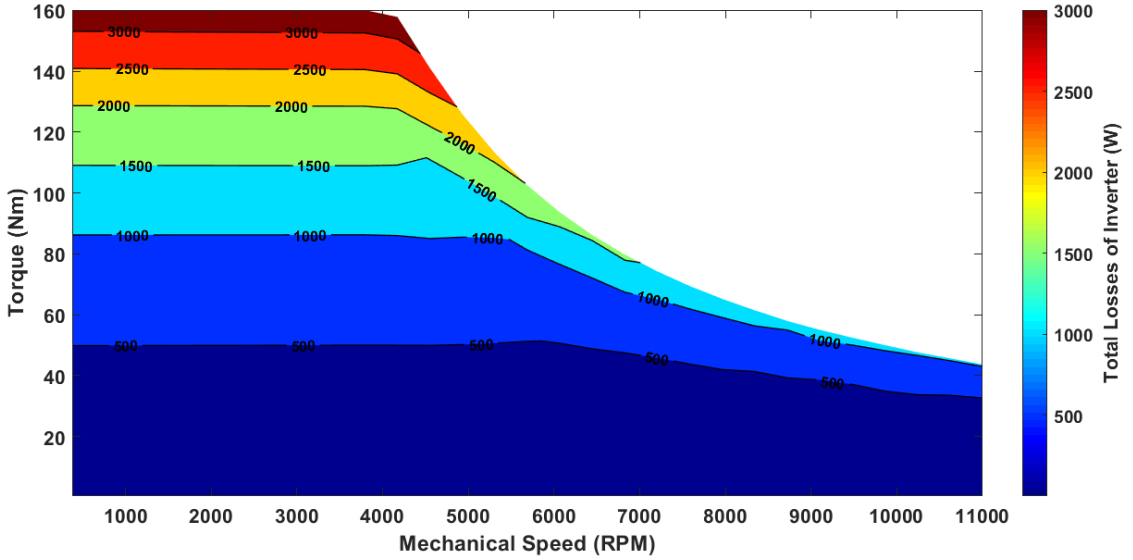

Figure 4.15: Total losses at all the operating points for FZ600R12KE3 IGBT inverter

A general observation that can be derived by observing the power loss results of FS600R07A2E3 and FZ600R12KE3 IGBT inverters is that the switching losses and conduction losses are comparable. Also, the increment of switching losses with respect to the increase in temperature is relatively high when compared to conduction losses. Therefore switching losses would become a limiting factor when it is required to operate the IGBT inverters at the high switching frequencies.

4.2.3 Visualization of phase current in MOSFET inverter during reverse conduction

Before calculating the power losses of SiC MOSFET inverter, it would be good to know how the current splits into MOSFET and its anti-parallel diode during the reverse conduction. Therefore visualizing the currents corresponding to MOSFETs and their anti-parallel diodes, in one of the phase legs, provides a better understanding of reverse conduction.

To show the plots of currents, another operating point is chosen, as shown in Table 4.6. The reason for choosing this operating point is that here the frequency of the sinusoidal currents and voltages is not much less than the frequency of the carrier wave. This facilitates to see the pulses in the MOSFET and diode currents.

Table 4.6: Details of the chosen operating point

Name	Value
Torque	160.09 Nm
Electrical Speed	12144 RPM
i_{sd}	-460.42 A
i_{sq}	397 A
Current Magnitude	608 A
ψ_{sd}	-26.9mWb
ψ_{sq}	81.1mWb
Modulation index	0.759

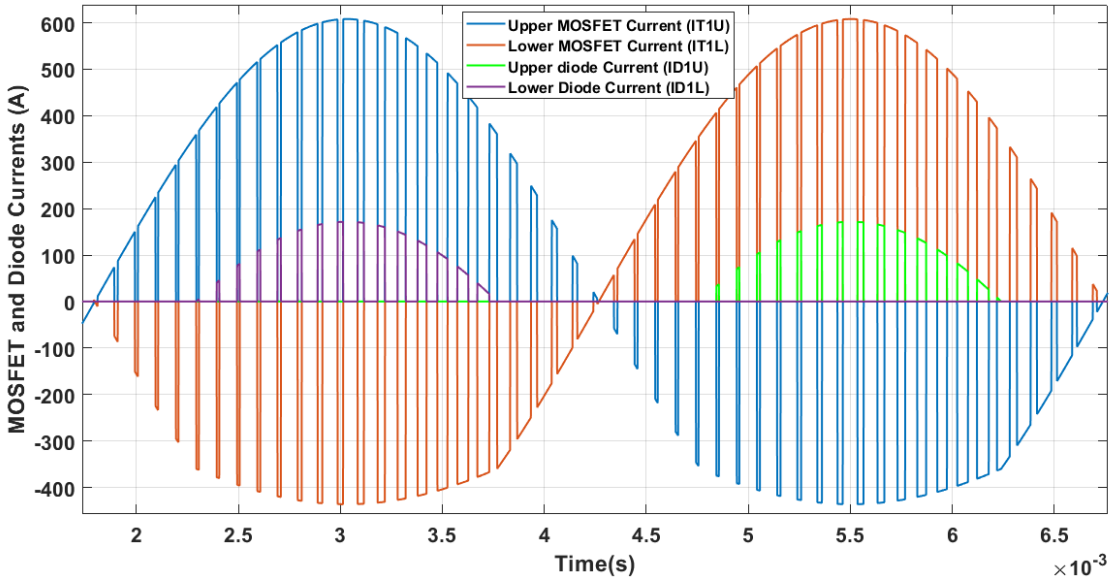

Figure 4.16: Current in MOSFETs and their anti-parallel diodes when the junction temperatures of both MOSFET and diode are 25°C

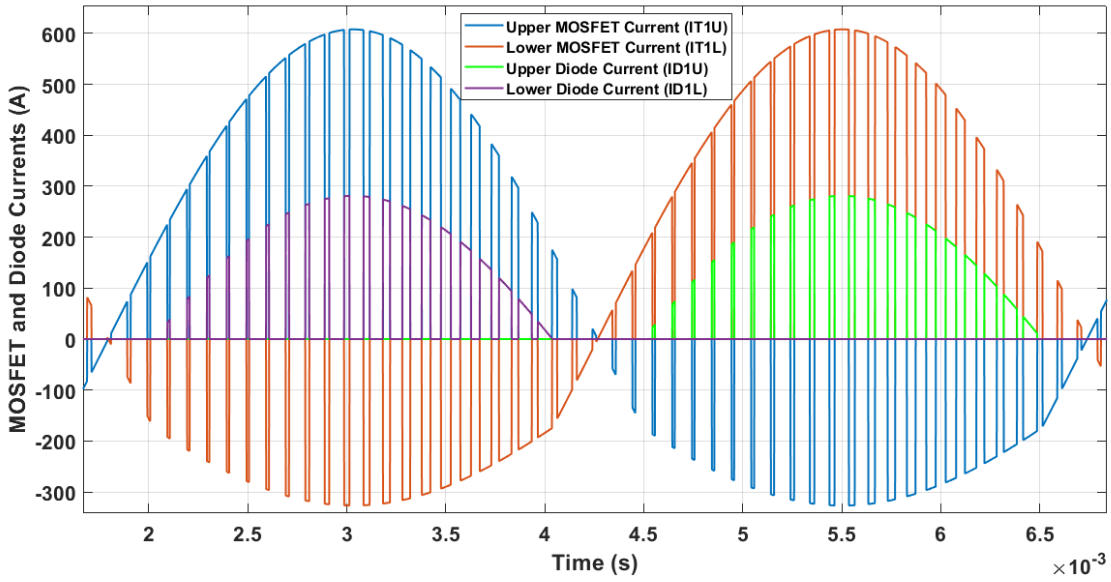

Figure 4.17: Current in MOSFETs and their anti-parallel diodes when the junction temperatures of both MOSFET and diode are 150°C

The current in MOSFETs and diodes of the first phase leg of the inverter are shown in Figs. 4.16 and 4.17. These figures show the phase current being split into MOSFETs and diodes, when MOSFET and diode junction temperatures are 25°C and 150°C respectively. When the junction temperature is 25°C, the diode's peak current value is around 172A, which is 28% of the phase current magnitude. Whereas, MOSFET's peak current value is around 436A, which is the remaining 72% of the phase current.

However, when the junction temperature is 150°C, 46% of the current flow into diode whereas the rest 54% of the current flows into MOSFET. It can be observed from these phase current share values that the part of the phase current flowing into MOSFET is reducing and the part that is flowing into the diode is increasing with the increase in junction temperature. This is because of higher on-state resistance of MOSFET when compared to its anti-parallel diode at high junction temperatures.

To explain the reverse conduction phenomenon at a lower current magnitude compared to the previous current, now the current magnitude is reduced to 427A, which in turn also means reduced torque demand, at the same electrical speed shown in Table 4.6.

Now due to the reduction in phase current magnitude, the peak value of diode current in Fig. 4.18 is 47A, which is just 7.7% of the phase current. This low current flow in the diode is because that with the reduction in current magnitude, the product of current and MOSFET's on-state resistance cannot be higher than the forward voltage of diode for a longer time in the fundamental half cycle, due to which the current tends to flow more into MOSFET than the diode. Fig. 4.19 shows the currents at $T_j = 150°C$, where it can be observed that more current flows into

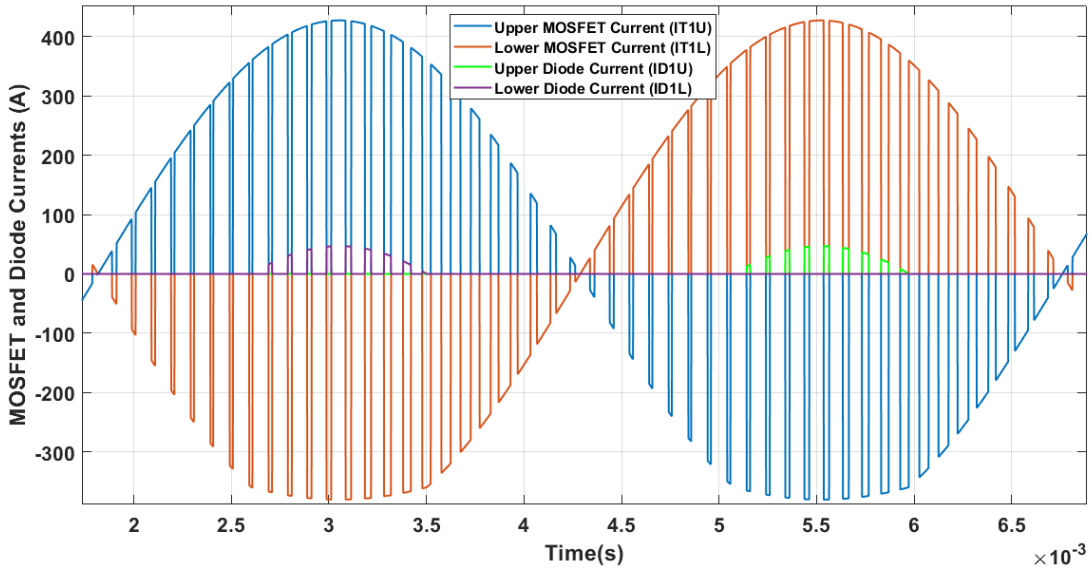

Figure 4.18: Current in MOSFETs and their anti-parallel diodes at $\hat{I} = 427$ A, when the junction temperatures of both MOSFET and diode are 25°C

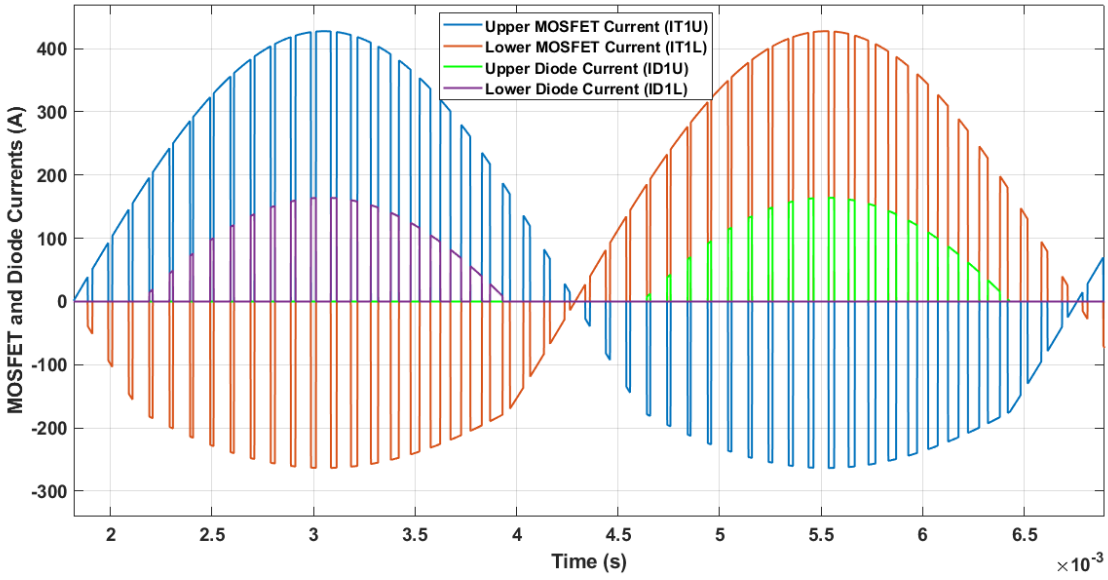

Figure 4.19: Current in MOSFETs and their anti-parallel diodes at $\hat{I} = 427$ A, when the junction temperatures of both MOSFET and diode are 150°C

diode now because of an increase of on-state resistance of MOSFET due to raise in temperature. This variation of current flow in diode and MOSFET due to raise in junction temperature is also reflected in the conduction power losses of MOSFET and diode, which is shown in the following section.

4.2.4 Power loss calculation and analysis of CAS300M12BM2 SiC MOSFET

The drain to source blocking voltage of CAS300M12BM2 SiC MOSFET is 1.2KV, and the nominal current rating is 300A. The current handling capability of SiC MOSFET is lesser when compared to Si IGBT because wafer process technology of SiC MOSFETs is still developing and large die size for high current carrying capability is not available at present [21]. Therefore, in this case, two CAS300M12BM2 half-bridge modules are connected in parallel in one leg such that at peak torque operating point either top or bottom switches of both modules together be able to carry the total current. For the comparison of power losses, the operating point mention in Table 4.1 is used.

In SiC MOSFETs it was observed that the rate of increase of on-state resistance with respect to junction temperature is relatively high when compared to that of Si IGBT. It was also seen that conduction losses of SiC MOSFET take a significant proportion of the total inverter losses since diode switching losses are zero and MOSFET switching losses are very low. Therefore in this section, conduction losses of MOSFET at different assumed junction temperatures are calculated to show the percentage increase of them, at a steady state.

Table 4.7: Total conduction losses of MOSFETs in CAS300M12BM2 inverter when reverse conduction is neglected in MOSFET

T_j **assumed (°C)**	**MOSFET cond.loss (W)**	T_j **actual (°C)**	**MOSFET cond. loss (W)**	**Diff.(W)**	**Diff.(%)**
65	869.61	74.65	908.52	38.9	4.47
75	909.97	85.01	953.52	43.54	4.78
85	953.42	95.40	1001.5	48.07	5.04
95	999.64	105.80	1052.3	52.65	5.26

Table 4.8: Total conduction losses of MOSFETs in CAS300M12BM2 inverter when reverse conduction is considered in MOSFET

T_j **assumed (°C)**	**MOSFET cond.loss (W)**	T_j **actual (°C)**	**MOSFET cond. loss (W)**	**Diff.(W)**	**Diff.(%)**
65	1268	76.81	1312.3	44.3	3.49
75	1306	87.15	1355.2	49.2	3.76
85	1347.2	97.51	1401.3	54.1	4.01
95	1391.3	107.89	1450.1	58.8	4.22

Table 4.9: Total conduction losses of IGBTs in FZ600R12KE3 IGBT inverter

T_j **assumed (°C)**	**IGBT cond.loss (W)**	T_j **actual (°C)**	**IGBT cond. loss (W)**	**Diff.(W)**	**Diff.(%)**
65	975.26	87.79	1009.6	34.33	3.52
75	990.30	98.41	1025.5	35.19	3.55
85	1005.4	109	1041.5	36.1	3.59
95	1020.4	119.64	1057.5	37.1	3.63

Tables 4.7 & 4.8 show the conduction losses of MOSFETs in inverter while neglecting and considering reverse conduction respectively. It can be observed from these two tables that reverse conduction in MOSFET considerably increases the conduction losses of MOSFET. Table 4.9 shows the total conduction losses of IGBTs in the inverter. T_j assumed column consists of the junction temperature values when the thermal design is still not implemented in the power loss calculations, that is when the junction temperature is considered equal to fluid temperature. Whereas T_j actual column consists of the junction temperature values at a steady-state, that is when the thermal design is implemented in power loss calculations as shown in Section 3.4.

In IGBT inverter at T_j assumed equals to 65°C, the steady-state junction temperature value obtained after thermal design implementation is 87.79°C, this means 22.79°C difference, which caused 34.33W increment in total IGBT conduction losses of the inverter. Whereas when T_j assumed equals to 95°C, the steady-state junction temperature value is 119.64°C, which means 24.64°C difference, and this caused an increment of 37.1W in total IGBT conduction losses of the inverter. Here it can be observed that increment of the conduction losses with respect to increasing junction temperature is linear, this is since the increment of on-state resistance of IGBT with respect to junction temperature raise is linear as shown in the Fig. 4.20

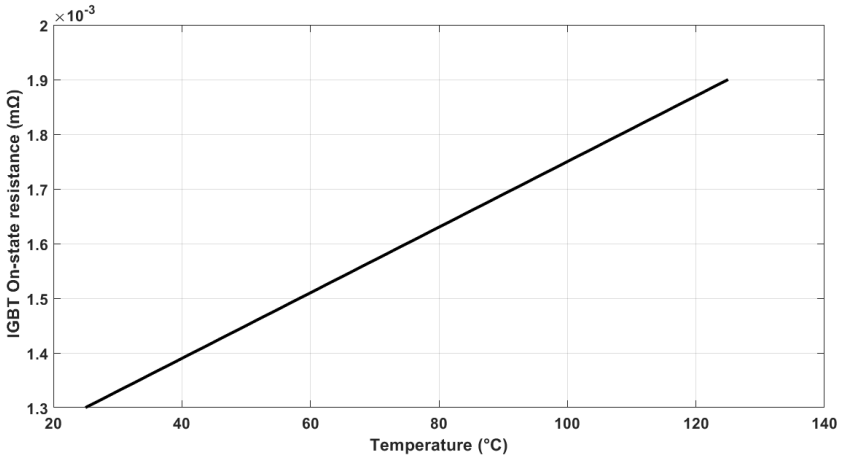

Figure 4.20: IGBT's on-state resistance Vs. Junction temperature

When reverse conduction is considered, see table 4.8, if the same analysis is done for the total MOSFET conduction losses of the inverter, the explanation is as follows. At T_j assumed equals to 65°C, the steady-state junction temperature of MOSFET is 76.81°C, this means 11.81°C, which caused 44.3 W increment in total MOSFET conduction losses of the inverter. Whereas when T_j assumed equals to 95°C, the steady-state junction temperature is 107.89°C, which means 12.89°C difference, and this caused an increment of 58.8W in total MOSFET conduction losses of the inverter. From the above values, it is understood that the increment of the conduction losses with respect to increase in junction temperature is not linear, this is because of the non-linear increment of on-state resistance of MOSFET with respect to increase in junction temperature as shown in the Fig. 4.21

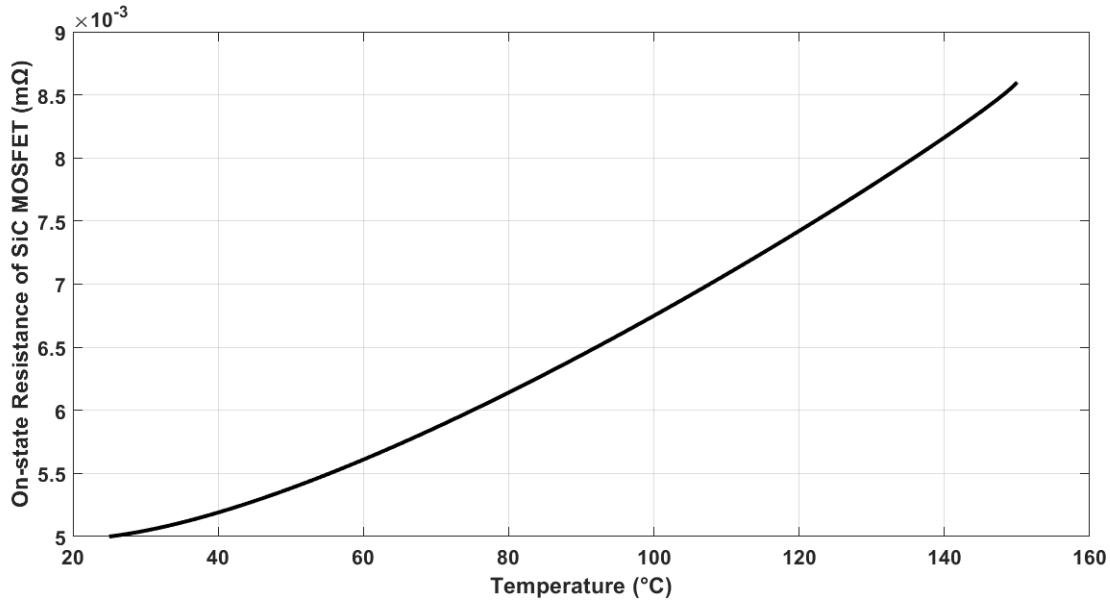

Figure 4.21: MOSFET's on-state resistance Vs. Junction temperature

The conduction losses of anti-parallel diodes of the SiC MOSFETs seem to increase linearly with respect to temperature because of the linear increase of diode's forward resistance with respect to junction temperature. However, the diode conduction losses seem to differ substantially when reverse conduction is considered in MOSFET.

Table 4.10: Total diode conduction losses without reverse conduction in MOSFET

T_j **assumed (°C)**	**Diode cond.loss (W)**	T_j **actual (°C)**	**Diode cond. loss (W)**	**Diff.(W)**	**Diff.(%)**
65	828.23	72.83	842.52	14.29	1.72
75	846.47	83.03	861.53	15.06	1.77
85	865.21	93.24	880.65	15.44	1.78
95	883.94	103.45	899.78	15.83	1.79

Table 4.11: Total diode conduction losses with reverse conduction in MOSFET

T_j **assumed** (°C)	**Diode cond.loss (W)**	T_j **actual** (°C)	**Diode cond. loss (W)**	**Diff.(W)**	**Diff.(%)**
65	132.55	68.06	147.72	15.16	11.44
75	145.26	78.22	161.58	16.31	11.23
85	158.51	88.39	175.85	17.33	10.93
95	172.18	98.56	190.45	18.27	10.61

Table 4.10 shows the total conduction power losses of diodes in the inverter, when thermal design is considered and neglected, while neglecting the reverse conduction in MOSFET, where Table 4.11 shows the same, but when reverse conduction is considered in MOSFET. It can be observed that reverse conduction in MOSFET substantially reduces the conduction losses in diodes.

For the accurate calculation of the total power loss of the module, switching losses have to be included. At the current magnitude shown in table 4.1, the switching loss was found to be 236 W. It was also observed that the variation of switching loss with respect to temperature is negligible. At T_j assumed equals to 65 °C and after implementing thermal design, the total losses of the SiC inverter is 1696 W, whereas the total losses of the FZ600R12KE3 IGBT inverter at the same conditions is 3288 W. Therefore MOSFET inverter is producing 1592 W less power loss than the IGBT inverter. The power that is saved by the MOSFET inverter is majorly because of less switching losses of MOSFETs and zero recovery loss of the anti-parallel diodes.

In the previous section, it was stated that with the increase in junction temperature of the MOSFET, more current flows into diode than MOSFET during reverse conduction, the reduction of current flow in MOSFET and increment of current flow in diode also affects the conduction power losses in a similar way as shown in Table 4.12.

Table 4.12: MOSFET and Diode conduction losses at T_j=25°C and T_j=150°C

$T_{j,MOSFET}$ (°C)	**MOSFET Cond. loss (W)**	$T_{j,MOSFET}$ (°C)	**MOSFET Cond. loss (W)**	**Diff.(W)**	**Diff.(%)**
25	1165	150	1684.5	519.5	44.59
$T_{j,Diode}$ (°C)	**Diode Cond. loss (W)**	$T_{j,Diode}$ (°C)	**Diode Cond. loss (W)**	**Diff.(W)**	**Diff.(%)**
25	94.95	150	254.01	159	167.45

It can be observed from the above table that due to increment in the junction temperature of MOSFET, its conduction losses are increased by only 44.59%, whereas diode conduction losses are increased by 167.45%, this is due to the increment of on-state resistance of the MOSFET with temperature, because of which the percentage current flow in MOSFET reduces, and in diode it increases.

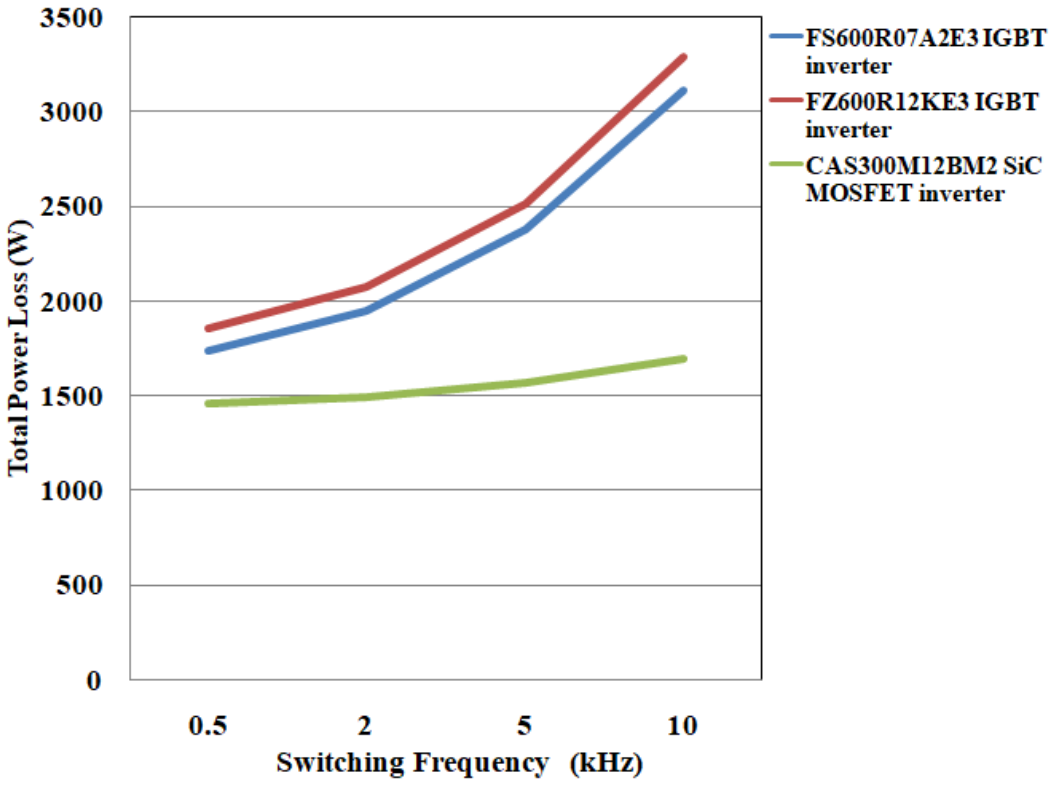

Figure 4.22: Total power losses of IGBT and SiC MOSFET inverters at different switching frequencies

The comparison of the total power losses of FS600R07A2E3, FZ600R12KE3 IGBT inverters and CAS300M12BM2 SiC MOSFET inverters at different switching frequencies are shown in Fig. 4.22, where it can be seen that total power losses of MOSFET inverter are not varying much with respect to switching frequency, whereas it varies a lot for IGBT inverters. The total power losses of IGBT and MOSFET inverters are in the range of comparison at lower switching frequencies, however, at higher switching frequencies SiC MOSFET inverter produce much lesser losses when compared to IGBT inverter. It can be seen that even FS600R07A2E3 IGBT inverter, which just has a blocking voltage of 650V, is producing more losses than MOSFET inverter which has a blocking voltage of 1200V. The lower increment of total losses of MOSFET inverter with respect to switching frequency is because of the lower switching energy of MOSFETs and zero recovery energy of diodes.

Finally the total losses of CAS300M12BM2 MOSFET inverter at all the operating points are shown in the Fig. 4.23, where it can be seen that the total losses at all

the operating points are less when compared to total losses of FS600R07A2E3 and FZ600R12KE3 inverters, shown in Figs. 4.13 and 4.15.

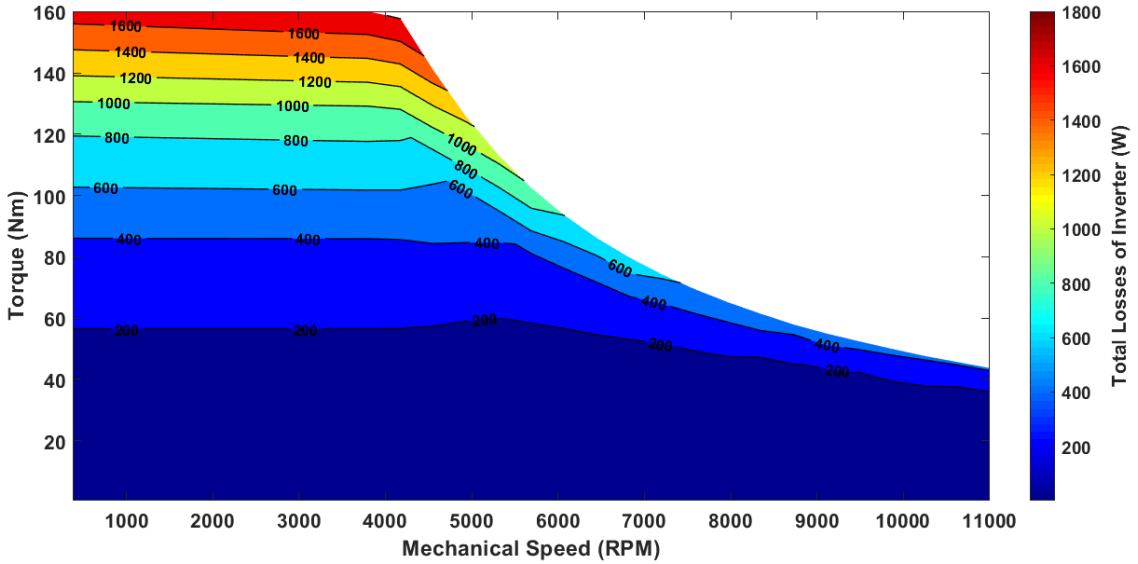

Figure 4.23: Total losses of CAS300M12BM2 SiC MOSFET inverter at steady-state, and all the operating points when T_j assumed equals to 65°C and $f_{sw} = 10kHz$

4.3 Comparison of Analytical and Numerical Results

To verify the results obtained using analytical equations provided in Section 3.3, the power losses are also calculated numerically in Matlab. The phase to neutral PWM voltage signal is obtained by comparing the three-phase control voltage signals, obtained from the current controller with a triangular carrier wave of 10KHz frequency. The identification of active IGBTs or MOSFETs and their anti-parallel diodes, magnitudes of the current flowing through them, during the fundamental period, is done based on the polarities of phase to neutral voltage u_m and phase current i_{ph} as discussed in the Section 3.2.

The frequencies of control voltage and current signals are obtained from the angular electrical speed of the PMSM. The conduction power losses, for two fundamental periods, of one FZ600R12KE3 IGBT and one CAS300M12BM2 SiC MOSFET at the operating shown in Table 4.1 are as shown in the Figs. 4.24 and 4.25. Whereas the comparison of analytical and numerical results of conduction and switching losses of the whole IGBT and MOSFET inverter are shown in the Tables 4.13 and 4.14.

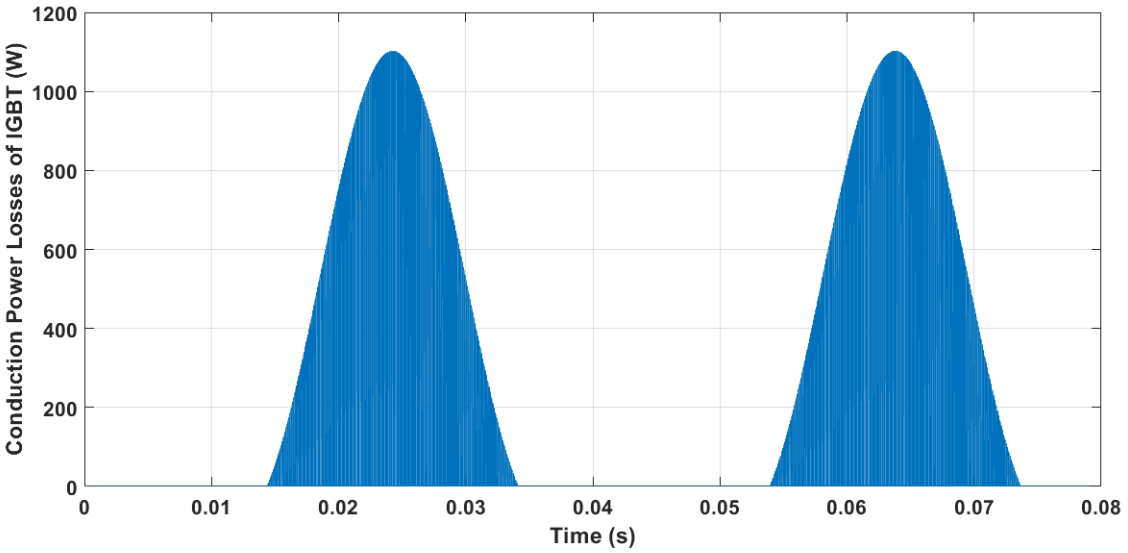

Figure 4.24: Conduction power losses of one of the IGBTs in a phase leg

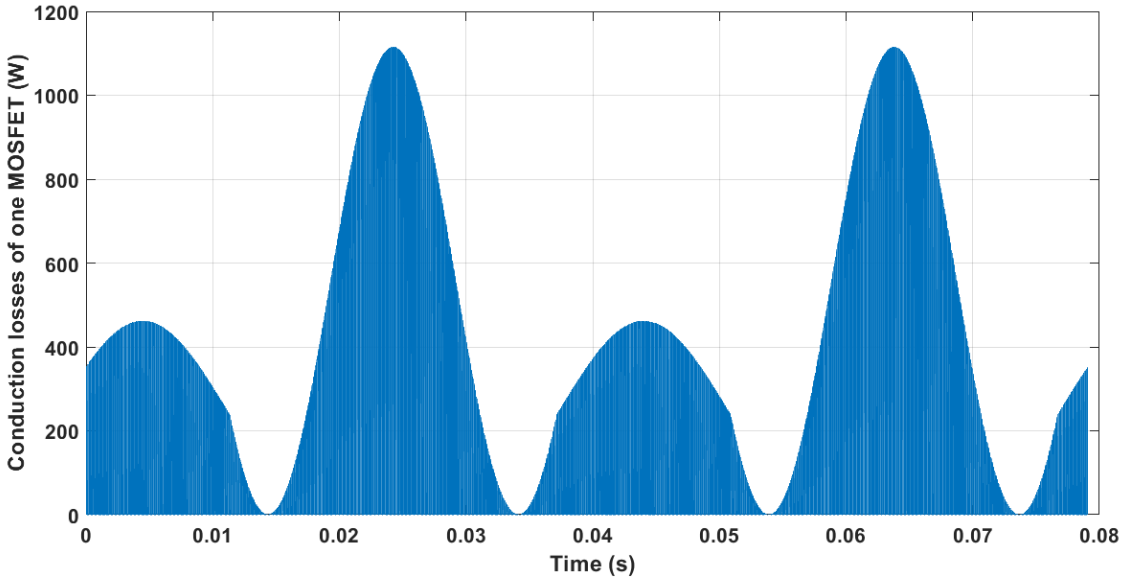

Figure 4.25: Conduction power losses of one of the MOSFETs in a phase leg

The average value of the conduction power loss is obtained by calculating the mean value of the losses present at the instants shown in the above figures. Average switching power losses are obtained by summing up the switching energies at all turn-on and turn-off instants of the devices.

Table 4.13: Comparison of analytical and numerical results of FZ600R12KE3 IGBT

Name	**Analytical Losses (W)**	**Numerical Losses (W)**	**Diff.(W)**	**Diff.(%)**
IGBT conduction loss	1009.6	1011.6	2	0.19
IGBT switching loss	927.06	927.23	0.17	0.01
Diode conduction loss	788.50	786.59	-1.90	-0.24
Diode switching loss	562.88	562.81	-0.07	-0.01
Total loss	3288	3288.2	0.2	0.006

Table 4.14: Comparison of analytical and numerical results of CAS300M12BM2 SiC MOSFET

Name	**Analytical Losses (W)**	**Numerical Losses (W)**	**Diff.(W)**	**Diff.(%)**
MOSFET conduction loss	1319.4	1312.3	-7.1	-0.53
MOSFET switching loss	236	236.1	0.1	0.04
Diode conduction loss	150.14	147.72	-2.42	-1.61
Diode switching loss	0	0	0	0
Total loss	1705.54	1696	-9.54	-0.55

The power losses calculated, by using analytical equations and by numerical results are almost same.

4.4 Power Losses of the Inverters with the Third Harmonic Injection

The power losses using THIPWM are calculated by using the operating point mentioned in Table 4.6 and the results are shown in Tables 4.15 and 4.16.

The reference voltages before and after the THIPWM are shown in Fig. 4.26.

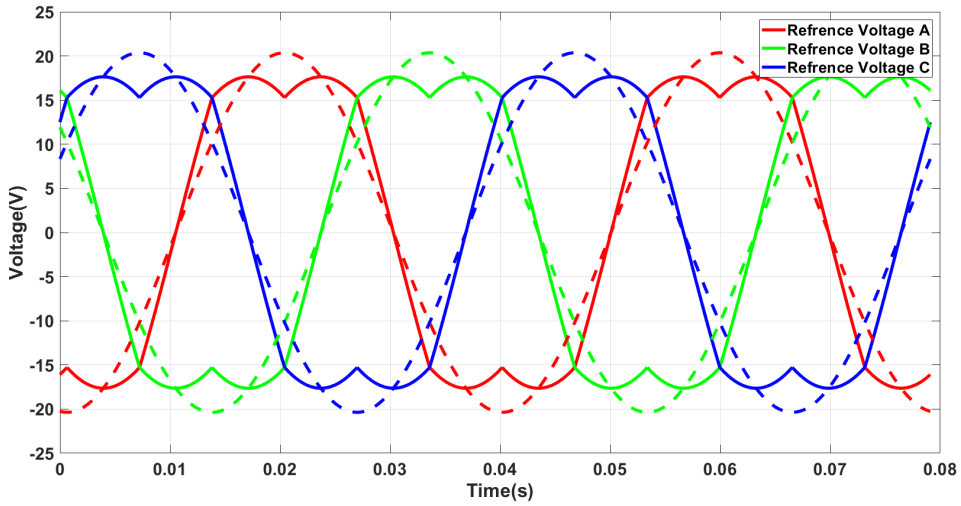

Figure 4.26: Three phase reference voltages with the third harmonic injection

The difference between the power losses with and without THIPWM are presented in Tables 4.15 and 4.16 for the FZ600R12KE3 Si IGBT inverter and CAS300M12BM2 SiC MOSFET inverter respectively.

Table 4.15: Power losses of the FZ600R12KE3 Si IGBT inverter before and after the third harmonic injection

Name	**Losses (W) before 3rd harmonic**	**Losses (W) after 3rd harmonic**	**Diff.(W)**	**Diff.(%)**
IGBT conduction loss	1011.6	1001.8	-9.8	-0.97
IGBT switching loss	927.23	927.33	0.09	0.001
Diode conduction loss	786.59	795.8	9.2	1.16
Diode switching loss	562.76	562.87	0.11	0.01
Total loss	3288.2	3287.7	-0.5	-0.01

Table 4.16: Power losses of the CAS300M12BM2 SiC MOSFET inverter before and after the third harmonic injection

Name	**Losses (W) before 3rd harmonic**	**Losses (W) after 3rd harmonic**	**Diff.(W)**	**Diff.(%)**
MOSFET conduction loss	1312.3	1308.3	-4	-0.30
MOSFET switching loss	236	236	0	0
Diode conduction loss	147.72	149.27	1.55	1.05
Diode switching loss	0	0	0	0
Total loss	1696	1693.6	-2.4	-0.14

It can be observed in Table 4.15, that the total power loss obtained using a pure sinusoidal PWM and THIPWM are almost same; this is since, the parameters, like the phase current and the DC-link voltage, on which the conduction and switching losses depend, remain unchanged even after the third harmonic signal injection in the reference voltages. The power loss results of the CAS300M12BM2 SiC MOSFET inverter also doesn't show much variation in the power loss, which can be seen in

Table 4.16, because of the same reasons mentioned for the FZ600R12KE3 Si IGBT inverter.

4.5 Results of the Life-Cycle Cost Analysis

The LCCA model, described in Section 3.6, is used to calculate the life-cycle cost of the CAS300M12BM2 SiC MOSFET inverter and FZ600R12KE3 IGBT inverter. Unlike in Section 4.2.4, here only one SiC MOSFET is considered instead of two in parallel; this is since the torque requirement in the driving cycle considered is low enough for the phase current to be lower than the rated current of the device, which is 300A. Therefore only three MOSFET modules are enough to build the inverter since each module consists of two positions. However, six FZ600R12KE3 IGBT modules are required, since each module consists of only one position.

By using the method described in Section 3.6, the NPV of the energy losses is calculated and presented in Table 4.17. It can be seen that the SiC MOSFET inverter causes 299.4 kWh of energy loss per year, whereas the Si IGBT inverter causes 517.7 kWh energy loss per year. The energy loss per year is converted into money for the energy cost analysis by multiplying the energy losses per year with the estimated unit price of the electricity in Sweden, C_{eng}.

To calculate the NPV, (3.36) is used and the lifetime of both the CAS300M12BM2 SiC MOSFET inverter and the FZ600R12KE3 Si IGBT inverter is considered to be 20 years. The NPV of the total energy loss for the lifetime of the SiC MOSFET inverter is found to be 14,002 kr, which is 42.16% lower than that of the Si IGBT inverter.

Table 4.17: Net Present Value of the energy losses

Power converter	**Energy loss per year (kWh)**	**Energy cost per year (kr)**	**NPV of 20 years (kr)**
CAS300M12BM2 SiC MOSFET inverter	299	898	14,002
FZ600R12KE3 Si IGBT inverter	517	1,553	24,212

The annual energy losses of the power converters are calculated by using the ECE driving cycle profile and the loss calculation equations for the power inverters are mentioned in Section 3.3. The losses of the SiC MOSFET inverter are calculated by considering reverse conduction and after the implementation of the thermal design.

Table 4.18 shows the total initial cost of the inverter modules and the cost of the cooling system components for both the SiC MOSFET and Si IGBT inverters. The cooling system is designed based on the total power losses of the converters mentioned in Tables 4.15 and 4.16. It can be seen from these tables that the SiC

MOSFET inverter has lower losses compared to the Si IGBT inverter; that's why the heat exchanger required for the heat dissipation of the SiC MOSFET inverter is less expensive than that for the Si IGBT inverter.

Table 4.18: Total Initial Cost of the CAS300M12BM2 SiC MOSFET inverter and FZ600R12KE3 Si IGBT inverter

Power converter	**Inverter price (kr)**	**Cooling System (kr)**	**Total Cost (kr)**
CAS300M12BM2 SiC MOSFET inverter	1,6325	1,500	17,825
FZ600R12KE3 Si IGBT inverter	7,743	2,000	9,743

Table 4.19, shows the life-cycle cost over 20 years of life time of the inverters. The power loss in terms of money, in the high-cost scenario, over the span of 50 years is shown in Fig. 4.27, which also shows the break-even point from which the usage of the SiC MOSFET inverter becomes beneficial.

Table 4.19: Summary of LCCA in high cost scenario

Power Converters	**Initial Cost (kr)**	**NPV of Energy losses (kr)**	**Total Cost (kr)**
CAS300M12BM2 SiC MOSFET inverter	17,825	14,002	31,827
FZ600R12KE3 Si IGBT inverter	9,743	24,212	33,955

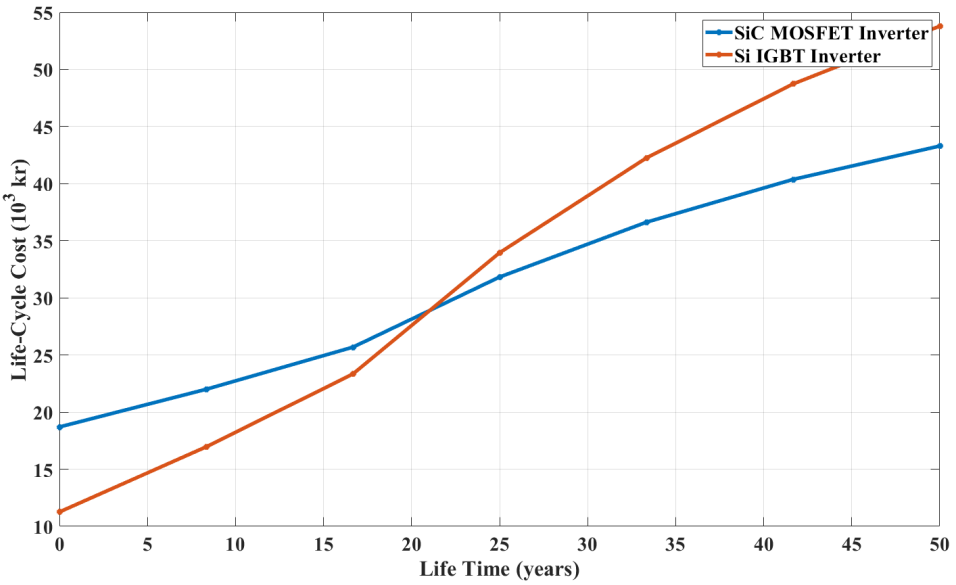

Figure 4.27: High cost scenario of the LCCA showing the power wastage in terms of money over the span of 50 years, where the break over point can be observed around 21 years

At present, the SiC MOSFET inverter is more expensive than the Si IGBT inverter due to the factors such as design limitations and limited availability in the market but if it is assumed that the SiC MOSFET inverter and Si IGBT inverter have same purchase price in the future, then the final results of the LCCA are presented in Table 4.20. The low-cost scenario of the LCCA showing the power wastage in terms of money over the span of 50 years is shown in Fig. 4.28, which shows that the SiC MOSFET inverter has a clear advantage over the Si IGBT inverter in terms of total cost and becomes more cost-competitive as the operational life of the device is increased further.

Table 4.20: Summary of LCCA in low cost scenario

Power Converters	**Initial Cost (kr)**	**NPV of Energy losses (kr)**	**Total Cost (kr)**
CAS300M12BM2 SiC MOSFET inverter	9,743	14,002	23,745
FZ600R12KE3 Si IGBT inverter	9,743	24,212	33,955

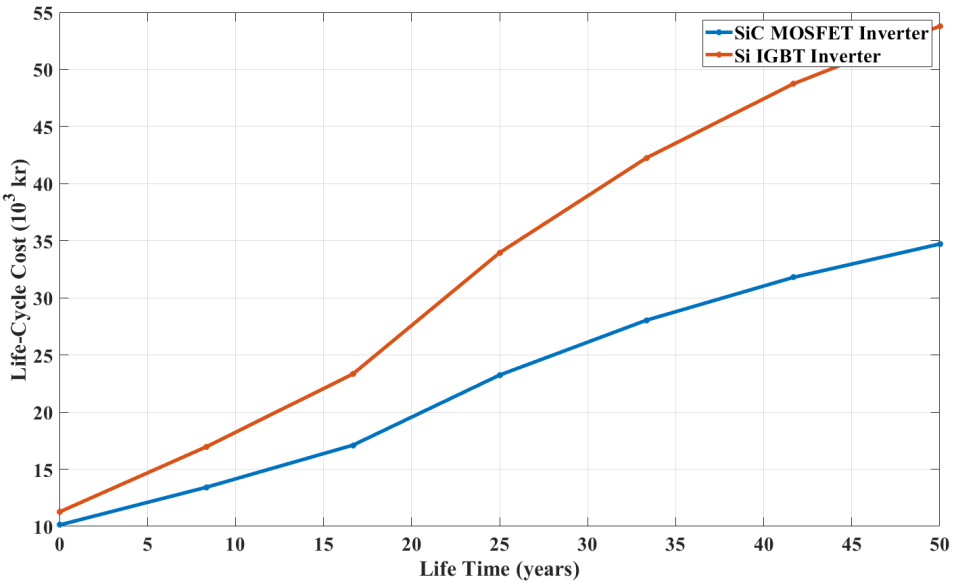

Figure 4.28: Low cost scenario of the LCCA showing the power wastage in terms of money over the span of 50 years

5
Conclusion

In this thesis work, a control system is developed for a non-linear permanent magnet synchronous motor. The strategies of MTPA and MTPV were implemented while generating the current references, and the result of this implementation is reflected in the currents drawn by the motor. For low torque demand, it was observed that the motor operates in the MTPA region for a large range of speeds when compared to the situation where the torque demand is high. It was also observed that when torque demand is high, to make the motor run at higher speeds, the torque demand has to be reduced.

The second part of the thesis work shows the comparisons of the power losses of IGBT and MOSFET inverters while considering and neglecting the thermal design implementation. At the chosen operating point, in IGBT inverters, it was observed that total switching losses are comparable with the total conduction losses and the switching loss increment with respect to temperature is more rapid when compared to conduction losses. At 0.5kHz switching frequency, the power losses of the SiC MOSFET inverter are 21% lower compared to that of the FZ600R12KE3 IGBT inverter, whereas this difference has increased to 48% at 10kHZ switching frequency. The rapid increment of the total power loss of the IGBT inverter with respect to the switching frequency is due to the rapid increment of the switching power loss.

In MOSFET inverters, even though that reverse conduction helps in reducing the conduction losses and thereby the total losses of the inverter, yet it was observed that the conduction losses of the MOSFETs are increasing more rapidly with the junction temperature raise. At the considered operating point, and at a junction temperature of 25°C, it was observed that 72% of the phase current flows into the MOSFET whereas the rest, 28% of the phase current flows into its anti-parallel diode. However, when the junction temperature is 150°C, it was observed that the percentage of the phase current that flows into the MOSFET has been reduced to 54% whereas it has increased to 46% in the anti-parallel diode. This variation in current flow with respect to the junction temperature of the devices has also affected the power losses.

In the high-cost scenario, the LCCA model developed, has shown that the usage of a SiC MOSFET inverter becomes advantageous after around 21 years. However, it was seen that in the low-cost scenario, a SiC MOSFET inverter has a clear advantage over the IGBT inverter just from the time of installation or usage.

Finally, it can be concluded that the usage of SiC MOSFETs is more advantageous when the switching frequency is high. SiC MOSFET inverter is more cost-saving over its lifetime if the initial cost of the SiC devices goes down. Otherwise, in the

present high-cost scenario, there is no substantial difference in the life cycle cost of both SiC MOSFET and Si IGBT inverter over a defined lifetime.

6
Future Work

In this thesis work, a control system is developed for a PMSM, and power losses of the drive system's inverter are evaluated, for all speed-torque combinations that this PMSM can operate.

The power loss calculations are done by considering sinusoidal and third harmonic injection PWM techniques. Different PWM techniques like space vector PWM and discontinuous PWM be implemented to check how the power losses vary.

The power loss and junction temperature calculations are valid for steady-sate conditions only. If the power losses vary with time then thermal impedance model has to be considered instead of thermal resistance model.

In LCCA analysis, operational and disposal costs could be included to have better LCCA model. There are different semiconductor devices from a variety of manufacturers, so the cost-effectiveness of various designs in converter modeling can be investigated.

Bibliography

[1] T. Gustafsson and A. Johansson, "Comparison between battery electric vehicles and internal combustion engine vehicles fueled by electrofuels," *Chalmers Tekniska HöGskola: Göteborg, Sweden*, 2015.

[2] W. Khan *et al.*, "Torque maximizing and flux weakening control of synchronous machines," 2016.

[3] L. Chedot and G. Friedrich, "A cross saturation model for interior permanent magnet synchronous machine. application to a starter-generator," in *Conference Record of the 2004 IEEE Industry Applications Conference, 2004. 39th IAS Annual Meeting.*, vol. 1, IEEE, 2004.

[4] A. Elasser, T. P. Chow, *et al.*, "Silicon carbide benefits and advantages for power electronics circuits and systems," *Proceedings of the IEEE*, vol. 90, no. 6, pp. 969–986, 2002.

[5] X. Ding, M. Du, T. Zhou, H. Guo, C. Zhang, and F. Chen, "Comprehensive comparison between sic-mosfets and si-igbts based electric vehicle traction systems under low speed and light load," *Energy Procedia*, vol. 88, pp. 991–997, 2016.

[6] M. Meyer, T. Grote, and J. Bocker, "Direct torque control for interior permanent magnet synchronous motors with respect to optimal efficiency," in *2007 European Conference on Power Electronics and Applications*, pp. 1–9, IEEE, 2007.

[7] M. Meyer and J. Bocker, "Optimum control for interior permanent magnet synchronous motors (ipmsm) in constant torque and flux weakening range," in *2006 12th International Power Electronics and Motion Control Conference*, pp. 282–286, IEEE, 2006.

[8] M. Rousselle, "Impact of the electric vehicle on the electric system," 2009.

[9] D.-P. Sadik, *On reliability of SiC power devices in power electronics*. PhD thesis, KTH Royal Institute of Technology, 2017.

[10] M. Nawaz and K. Ilves, "Replacing si to sic: Opportunities and challenges," in *2016 46th European Solid-State Device Research Conference (ESSDERC)*, pp. 472–475, IEEE, 2016.

[11] V. Benda, "Power semiconductors—state of art and future trends," in *AIP Conference Proceedings*, vol. 1337, pp. 16–24, AIP, 2011.

[12] C. Mademlis and V. G. Agelidis, "On considering magnetic saturation with maximum torque to current control in interior permanent magnet synchronous motor drives," *IEEE transactions on energy conversion*, vol. 16, no. 3, pp. 246–252, 2001.

[13] B. Ozpineci and L. M. Tolbert, "Characterization of sic schottky diodes at different temperatures," *IEEE Power Electronics Letters*, vol. 1, no. 2, pp. 54–57, 2003.

[14] L. M. Tolbert, B. Ozpineci, S. K. Islam, and F. Z. Peng, "Impact of sic power electronic devices for hybrid electric vehicles," tech. rep., SAE Technical Paper, 2002.

[15] K. Nagasai and T. Jyothsna, "Harmonic analysis and application of pwm techniques for three phase inverter," *International Research Journal of Engineering and Technology (IRJET) Volume*, vol. 3, 2016.

[16] H. Li, L. Qu, and W. Qiao, "Life-cycle cost analysis for wind power converters," in *2017 IEEE International Conference on Electro Information Technology (EIT)*, pp. 630–634, IEEE, 2017.

[17] D. Galar, P. Sandborn, and U. Kumar, *Maintenance costs and life cycle cost analysis*. CRC Press, 2017.

[18] A. Acquaviva and T. Thiringer, "Energy efficiency of a sic mosfet propulsion inverter accounting for the mosfet's reverse conduction and the blanking time," in *2017 19th European Conference on Power Electronics and Applications (EPE'17 ECCE Europe)*, pp. P–1, IEEE, 2017.

[19] R. Künzi, "Thermal design of power electronic circuits," CERN.

[20] H. Gaspars-Wieloch, "Project net present value estimation under uncertainty," *Central European Journal of Operations Research*, vol. 27, no. 1, pp. 179–197, 2019.

[21] S. Yin, K. J. Tseng, R. Simanjorang, and P. Tu, "Experimental comparison of high-speed gate driver design for 1.2-kv/120-a si igbt and sic mosfet modules," *IET Power Electronics*, vol. 10, no. 9, pp. 979–986, 2017.

A

Appendix

Algorithm to obtain all the operating points are shown in Figs. A.1 and A.2

```
% Deriving MTPA and MTPV points at full/maximum torque
for i=1:length(Wr)

    Usd=(Rs.*Isd)-((Wr(i)).*Psiq);      %deriving d axis voltage
    Usq=(Rs.*Isq)+((Wr(i)).*Psid);      %deriving q axis voltage

    Uamp=sqrt((Usd.^2)+(Usq.^2));       %Deriving voltage amplitude

    temp= (Uamp <= Umax)&(Iamp <= Imax); %current and voltage filtering outside the machine & inverter ratings

    Iamp_temp=Iamp(temp);     %Storing all the Iamp values where temp=1 i.e where (Uamp <= Umax)&(Iamp <= Imax) is
    Isd_temp=Isd(temp);       %Storing all the Isd values where temp=1
    Isq_temp=Isq(temp);       %Storing all the Isq values where temp=1
    Psid_temp=Psid(temp);     %Storing all the Psid values where temp=1
    Psiq_temp=Psiq(temp);     %Storing all the Psiq values where temp=1
    T_em_temp=T_em(temp);     %Storing all the T_em values where temp=1

    %maximum torque
    %index varaible stores the index values of max torques
    [T_em_max(i),index]= max(T_em_temp); %Storing all max values of T_em_temp i.e storing all max torque values at
    Isd_index(1,i)=Isd_temp(index);      % Storing Isd_temp values of the index numbers, where the maximum torque l
    Isq_index(1,i)=Isq_temp(index);      % Storing Isq_temp values of the index numbers, where the maximum torque l
    T_em_index(1,i)=T_em_temp(index);    % Storing T_em_temp values of the index numbers, where the maximum torque
    Psid_index=Psid_temp(index);         % Storing Psid_temp values of the index numbers, where the maximum torque
    Psiq_index=Psid_temp(index);         % Storing Psiq_temp values of the index numbers, where the maximum torque
end
```

Figure A.1: For loop to obtain all the operating at full torque demand

```
T_em_max_res = linspace(0*max(T_em_max),0.9*max(T_em_max),10); %Creating range of torques i.e 0 to 90% of full torque

for j=length(T_em_max_res):-1:1   %creating for loop for 0 to 90% of full torque

    for i=1:length(Wr)            %creating for loop for speed vector

        Usd=(Rs.*Isd)-((Wr(i)).*Psiq);              %Same procedure as previous for loop
        Usq=(Rs.*Isq)+((Wr(i)).*Psid);
        Uamp=sqrt((Usd.^2)+(Usq.^2));
        temp = (Uamp <= Umax)&(Iamp <= Imax);
        Iamp_temp=Iamp(temp);
        Isd_temp =Isd(temp);
        Isq_temp =Isq(temp);
        T_em_temp=T_em(temp);
        temp = (T_em_temp >= 0.1*(10-j)*T_em_max(i)); %Removing the values which lie below the present torque range and s
        Iamp_temp=Iamp_temp(temp);
        Isd_temp =Isd_temp(temp);
        Isq_temp =Isq_temp(temp);
        T_em_temp =T_em_temp(temp);
        [~,index]=min(Iamp_temp);                   %Storing the index numbers of minimum current values
        Isd_index(j+1,i)=Isd_temp(index);
        Isq_index(j+1,i)=Isq_temp(index);
        T_em_index(j+1,i)=T_em_temp(index);

        fprintf('j = %d   i = %d   I_s_d = %.2f   I_s_q = %.2f   T_em = %.2f \n\n',j,i,Isd_index(j+1,i),Isq_index(j+1,i),'
```

Figure A.2: For loop to obtain all the operating points from 0 to 90 percent of full torque demand